

WL-TR-93-4029

PHOTO-ASSISTED EPITAXIAL GROWTH
FOR III-V SEMICONDUCTORS

420
900

AD-A267 889



C.W.TU

DEPT OF ELECTRICAL & COMPUTER ENGINEERING
UNIVERSITY OF CALIFORNIA, SAN DIEGO
LA JOLLA CA 92093-0407

FEB 1993

INTERIM REPORT FOR 09/01/90-10/31/92

APPROVED FOR PUBLIC RELEASE; DISTRIBUTION IS UNLIMITED.

DTIC
ELECTE
AUG 12 1993
S B D

93-18657



58,41


MATERIALS DIRECTORATE
WRIGHT LABORATORY
AIR FORCE MATERIEL COMMAND
WRIGHT PATTERSON AFB OH 45433-7734

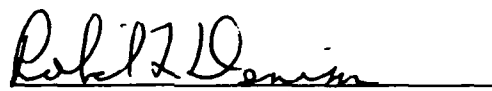
NOTICE


When government drawings, specifications, or other data are used for any purpose other than in connection with a definitely Government-related procurement, the United States Government incurs no responsibility or any obligation whatsoever. The fact that the government may have formulated or in any way supplied the said drawings, specifications, or other data, is not to be regarded by implication, or otherwise in any manner construed, as conveying any rights or permission to manufacture, use or sell any patented invention that may in any way be related thereto.

This report is releasable to the National Technical Information Service (NTIS). At NTIS, it will be available to the general public, including foreign nations.

This technical report has been reviewed and is approved for publication.


WILLIAM C. MITCHEL
Project Monitor
Electronic and Optical Matls. Branch


ROBERT L. DENISON, Chief
Electronic and Optical Matls. Branch
Electromagnetic Materials and
Survivability Division


WILLIAM R. WOODY, Chief
Electromagnetic Materials and Survivability Division
Materials Directorate
Wright Laboratory

If your address has changed, if you wish to be removed from our mailing list, or if the addressee is no longer employed by your organization, please notify WL/MLPO, WPAFB, OH 45433-current zip to help maintain a current mailing list.

Copies of this report should not be returned unless return is required by security considerations, contractual obligations, or notice on a specific document.

REPORT DOCUMENTATION PAGE			Form Approved OMB No. 0704-0188	
<small>Public reporting burden for this collection of information is estimated to average 1 hour per response, including the time for reviewing instructions, searching existing data sources, gathering and maintaining the data needed, and completing and reviewing the collection of information. Send comments regarding this burden estimate or any other aspect of this collection of information, including suggestions for reducing this burden, to Washington Headquarters Services, Directorate for Information Operations and Reports, 1215 Jefferson Davis Highway, Suite 1204, Arlington, VA 22202-4302, and to the Office of Management and Budget, Paperwork Reduction Project (0704-0188), Washington, DC 20503.</small>				
1. AGENCY USE ONLY (Leave blank)		2. REPORT DATE FEB 1993		3. REPORT TYPE AND DATES COVERED INTERIM 09/01/90--10/31/92
4. TITLE AND SUBTITLE PHOTO-ASSISTED EPITAXIAL GROWTH FOR III-V SEMICONDUCTORS			5. FUNDING NUMBERS C F33615-90-C-5946 PE 62102 PR 2423 TA 01 WU B7	
6. AUTHOR(S) W. TU				
7. PERFORMING ORGANIZATION NAME(S) AND ADDRESS(ES) DEPT OF ELECTRICAL & COMPUTER ENGINEERING UNIVERSITY OF CALIFORNIA, SAN DIEGO LA JOLLA CA 92093-0407			8. PERFORMING ORGANIZATION REPORT NUMBER UCSD-CWT-93-R1	
9. SPONSORING / MONITORING AGENCY NAME(S) AND ADDRESS(ES) MATERIALS DIRECTORATE WRIGHT LABORATORY AIR FORCE MATERIEL COMMAND WRIGHT PATTERSON AFB OH 45433-7734			10. SPONSORING / MONITORING AGENCY REPORT NUMBER WL-TR-93-4029	
11. SUPPLEMENTARY NOTES				
12a. DISTRIBUTION / AVAILABILITY STATEMENT APPROVED FOR PUBLIC RELEASE; DISTRIBUTION IS UNLIMITED.			12b. DISTRIBUTION CODE	
13. ABSTRACT (Maximum 200 words) Photo-assisted metalorganic molecular beam epitaxy (MOMBE), with an argon ion laser, has been used to grow GaAs. The substrate temperature was calibrated by an infrared laser interferometric technique with an accuracy of ± 3 °C. The MOMBE growth of GaAs, InAs, and InGaAs was first studied, by monitoring intensity oscillations of reflection high-energy electron diffraction (RHEED). The actual arsenic incorporation rate was deduced from As-induced RHEED oscillations, and a unity V/III incorporation ratio could be obtained. In growing InGaAs, indium segregation suppresses the InGaAs growth rate. In laser-assisted MOMBE the enhancement of arsenic desorption with laser irradiation and its effects were observed. The decomposition of triethylgallium and desorption of arsenic compete with each other, resulting in a saturation in the enhanced growth rate in the arsenic-controlled growth regime. The initial growth behavior was also studied by inspecting the details of the RHEED behavior and arsenic surface coverage.				
14. SUBJECT TERMS MOLECULAR BEAM EPITAXY, PHOTO-ASSISTED, METAL- ORGANICS GALLIUM ARSENIDE, INDIUM ARSENIDE, ARGON ION LASER			15. NUMBER OF PAGES 56	
			16. PRICE CODE	
17. SECURITY CLASSIFICATION OF REPORT UNCLASSIFIED	18. SECURITY CLASSIFICATION OF THIS PAGE UNCLASSIFIED	19. SECURITY CLASSIFICATION OF ABSTRACT UNCLASSIFIED	20. LIMITATION OF ABSTRACT UL	

Table of Contents

LIST OF FIGURES.....	iv
LIST OF TABLES.....	vi
1. INTRODUCTION.....	1
2. TECHNICAL RESULTS.....	3
2.1 Infrared Laser Interferometry.....	3
2.1.1 Principle of Operation.....	3
2.1.2 Substrate Temperature Calibration.....	4
2.1.3 Measurement of Ar Ion Laser Induced Local Heating.....	11
2.2 MOMBE Growth.....	16
2.2.1 Growth Study of GaAs and InAs by RHEED.....	16
2.2.2 Characterization of Epitaxial GaAs Layer.....	30
2.2.3 InGaAs Growth.....	30
2.3 Ar Ion Laser-Assisted MOMBE Growth.....	32
2.3.1 Laser-Enhanced Decomposition of TEGa.....	35
2.3.2 Laser-Enhancement of Arsenic Desorption and its Effect.....	39
2.3.3 The Initial Growth Behavior.....	44
2.3.4 Postgrowth Characterization.....	46
3. FUTURE WORK.....	48
4. REFERENCES.....	50

DTIC QUALITY INSPECTED 3

Accession For	
NTIS GRA&I	<input checked="checked" type="checkbox"/>
DTIC TAB	<input type="checkbox"/>
Unannounced	<input type="checkbox"/>
Justification	
By _____	
Distribution/	
Availability Codes	
Dist	Avail and/or Special
A-1	

LIST OF FIGURES

Fig. 1	The physics of interferometry	5
Fig. 2	The infrared laser interferometry setup in the annealing furnace	6
Fig. 3	Interferogram of 500- μm -thick GaAs sample by 1.15- μm He-Ne laser inside a furnace	8
Fig. 4	Temperature calibration curves for GaAs and InP samples by IR laser interferometry in a furnace	9
Fig. 5	Substrate heating power vs. sample temperature calibration in MBE growth chamber	10
Fig. 6	Measurement setup of substrate temperature change induced by Ar ion laser heating	12
Fig. 7	Interferogram of GaAs sample under 5-W Ar ion laser irradiation (a) without In attachment, clear oscillations during heating and cooling (b) with In attachment, unclear oscillations	13
Fig. 8	GaAs sample surface temperature increment versus Ar ion laser power output	15
Fig. 9	GaAs growth rate versus substrate temperature at different TEGa flow rate for an arsenic flux of 3.0×10^{-6} torr	18
Fig. 10	Growth rate versus TEGa flow rate at different substrate temperatures under an arsenic flux of 3.0×10^{-6} torr	19
Fig. 11	Growth rate versus TEGa flow rate at different substrate temperatures under an arsenic flux of 2.5×10^{-6} torr	21
Fig. 12	Growth rate versus TEGa flow rate at different substrate temperatures under an arsenic flux of 4.0×10^{-6} torr	22
Fig. 13	RHEED intensity oscillation data for (a) linear region, (b) transition region, and (c) stabilization region	23
Fig. 14	RHEED oscillations for MOMBE of GaAs using TEGa and arsenic. Both group-III and group-V induced oscillations are shown	25
Fig. 15	Arsenic-induced growth rate as a function of the substrate temperature at a TEGa flow of 0.35 sccm for different arsenic fluxes	27
Fig. 16	InAs growth rate as a function of TMIn flow rate	28
Fig. 17	InAs growth rate as a function of substrate temperature	29
Fig. 18	Low temperature (8K) photoluminescence measurement for GaAs epilayer	31

Fig. 19	Transient behavior of InGaAs growth rate. The decrease of growth rate is observed at higher TMIn flow rate	33
Fig. 20	RHEED oscillations with and without laser irradiation at a substrate temperature of 365°C. Enhanced growth of GaAs is observed with laser irradiation while no growth is observed without laser irradiation	37
Fig. 21	RHEED oscillations with and without Ar ion laser irradiation with TEGa and As supply at a substrate temperature of 410°C.....	38
Fig. 22	RHEED data showing arsenic desorption behavior under laser irradiation and arsenic exposure	40
Fig. 23	The growth rate of GaAs versus arsenic beam equivalent pressure under 4-W Ar ion laser irradiation at a substrate temperature of 390°C	42
Fig. 24	Growth rate versus Ar ion power at a constant TEGa flow but under different arsenic fluxes at a substrate temperature of 390°C	43
Fig. 25	The growth time of the first monolayer versus the Ar ion laser power under three different arsenic fluxes at a substrate temperature of 390°C	45
Fig. 26	The cross-section profile of the GaAs spot measured by Dektak stylus profiler	47
Fig. 27	LAMOMBE system	49

LIST OF TABLES

Table 1	The growth behavior of Ar ion laser-assisted GaAs grown in the substrate temperature range of 330°C-450°C	35
---------	---	----

1. INTRODUCTION

This is the interim report for the program undertaken in UCSD to develop a laser-assisted metalorganic molecular beam epitaxy (MOMBE) or chemical beam epitaxy (CBE) technique for the growth of III-V compound semiconductors. III-V compound semiconductors are important in a variety of high-performance electronic and optoelectronic applications. As a method that combines some of the advantages of molecular beam epitaxy (MBE) and metalorganic chemical vapor deposition (MOCVD), MOMBE/CBE provides some unique advantages, such as selective-area growth on patterned substrates and the ease in generating a large-area uniform beam. Photo-assisted MOMBE/CBE offers the additional advantage of selective-area epitaxy and doping without masks in a controlled environment at low substrate temperatures.

In Section 2.1, we report the use of an infrared laser interferometric technique to calibrate the substrate temperature with a higher accuracy. This technique is especially valuable for low substrate temperatures where the conventional pyrometer cannot be used and thermocouple is not accurate. This technique can also be used to measure the local temperature rise caused by Ar ion laser heating. The MOMBE growth study is described in Section 2.2. The growth of GaAs and InAs was studied extensively, and both the Ga-induced and As-induced growth were investigated. The actual arsenic incorporation rate was deduced from As-induced intensity oscillations of reflection high energy electron diffraction (RHEED), and a unity V/III incorporation ratio could be obtained. The experiment on the ternary compound InGaAs shows that indium segregation suppresses the InGaAs growth rate.

Ar⁺-laser-assisted MOMBE of GaAs was studied by monitoring the RHEED intensity oscillations, which forms part of Section 2.3. The enhancement of arsenic desorption with laser irradiation and its effect on laser-assisted MOMBE were observed. Both pyrolytic and photolytic decomposition of TEGa play roles in the surface chemical

reaction, and the decomposition of TEGa and desorption of arsenic compete with each other in laser-assisted MOMBE growth of GaAs, resulting in a saturation in the enhanced growth rate in the arsenic-controlled growth regime. The initial growth behavior was studied by inspecting the detail of the RHEED behavior and the arsenic surface coverage, and two growth mechanisms, physisorption and chemisorption, were proposed.

Finally, Section 3 lists some future work.

2. TECHNICAL RESULTS

2.1 Infrared Laser Interferometry

A precise temperature control during growth of thin films is necessary for optimizing the material characteristics. Thermocouples and optical pyrometers are widely used to measure the substrate temperature. Although accurate, the thermocouple needs to be in direct contact with the sample. One can avoid this problem by placing the thermocouple very close to the substrate holder. However, this method usually generates an uncertainty of $\pm 40^{\circ}\text{C}$ in an MBE system [1] due to radiation from the heater and reflection of radiation from the back of the substrate holder. On the other hand, the optical pyrometer is contactless and needs only the thermal radiation of the target [2-4]. Unfortunately, the pyrometer registers its signal from the absolute infrared (IR) radiation intensity, so the pyrometer cannot work for temperatures below 500°C . Furthermore, any coating on the viewport during growth or the existence of any other radiative sources within the growth chamber will decrease the accuracy of the detection [5,10].

Recently a contactless IR laser interferometry method was demonstrated to overcome the above problems in MOCVD and MBE growth of semiconductors [5-9]. This technique is particularly useful for us because laser-assisted MOMBE operates at low substrate temperatures. In our work we have used this technique to calibrate the substrate temperature from 25°C to 550°C and measure the temperature increase due to Ar^{+} laser irradiation.

2.1.1 Principle of Operation

An optical reflection will result upon the encountering of a difference in the refractive index. Because our samples are double-side-polished, both the front and the rear surfaces will act as reflective planes. The reflected beams from both the front and

the back surfaces of the wafer result in interference. The physical illustration of laser interferometry is shown in Fig. 1. For normal incidence, the phase difference between both reflected beams (R_1 and R_2) will be

$$\Phi = 2\pi \cdot (2/\lambda) \cdot n_2 \cdot f$$

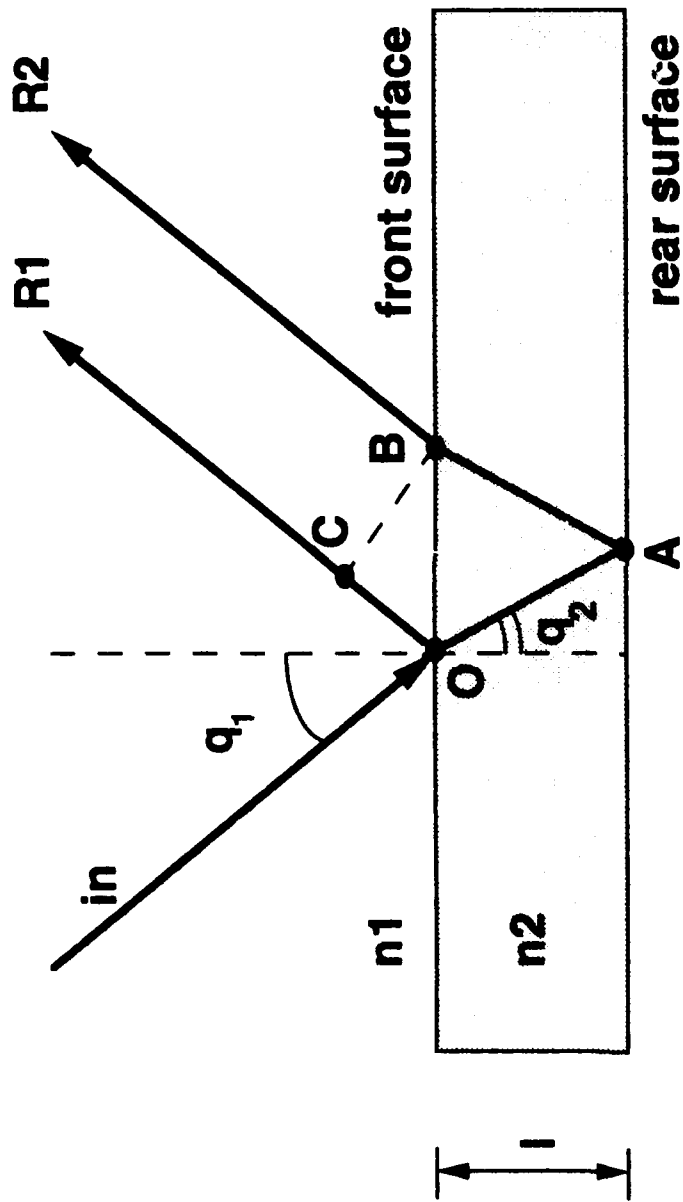
Where λ is the free space wavelength of the laser; n_2 the refractive index of the substrate; and f its thickness. We chose an infrared laser ($\lambda = 1.15 \mu\text{m}$) so that the substrate is transparent. Φ by itself has no significance, but it is its variation ($\Delta\Phi$) with respect to the temperature change (ΔT) that is important to our experiment. Since the change in substrate thickness due to thermal expansion is much smaller than λ , the effect of the temperature dependence of n_2 dominates. Therefore,

$$\Delta\Phi \approx (2\pi \cdot \frac{2}{\lambda} \cdot 1) \cdot \Delta n_2$$

As Δn_2 increases with temperature, $\Delta\Phi$ varies as well. Therefore, by keeping track of the number of maxima and minima on the interference pattern, one can find $\Delta\Phi$ and then the actual temperature variation (ΔT) away from the reference temperature (T_0).

2.1.2 Substrate Temperature Calibration

Since the actual temperature dependence of n_2 and f are too complicated to be described analytically, a theoretical prediction of $\Delta\Phi$ as a function of ΔT is not feasible. Therefore, we calibrated the dependence of $\Delta\Phi$ on ΔT experimentally (the dependence of the interferometric fringe number ΔN versus the change in sample temperature T_s) within an annealing furnace where a known, uniform temperature could be maintained. The measurement setup is shown in Fig. 2. A double-side-polished GaAs (500 μm thick) or InP (300 μm thick) substrate was clamped onto a sample holder and positioned at the center part of the annealing furnace. A 1.15- μm He-Ne laser was directed to the wafer at normal incidence, and the reflected beam was detected by a photodiode. The signal was amplified by our home-made amplifier circuit, and the interferogram was recorded by a



$R1$ = reflected beam from the front surface.
 $R2$ = reflected beam from the rear surface.
 $n1$ = refractive index of the surrounding.
 $n2$ = refractive index of the sample.
 l = thickness.

Fig. 1 The physics of interferometry

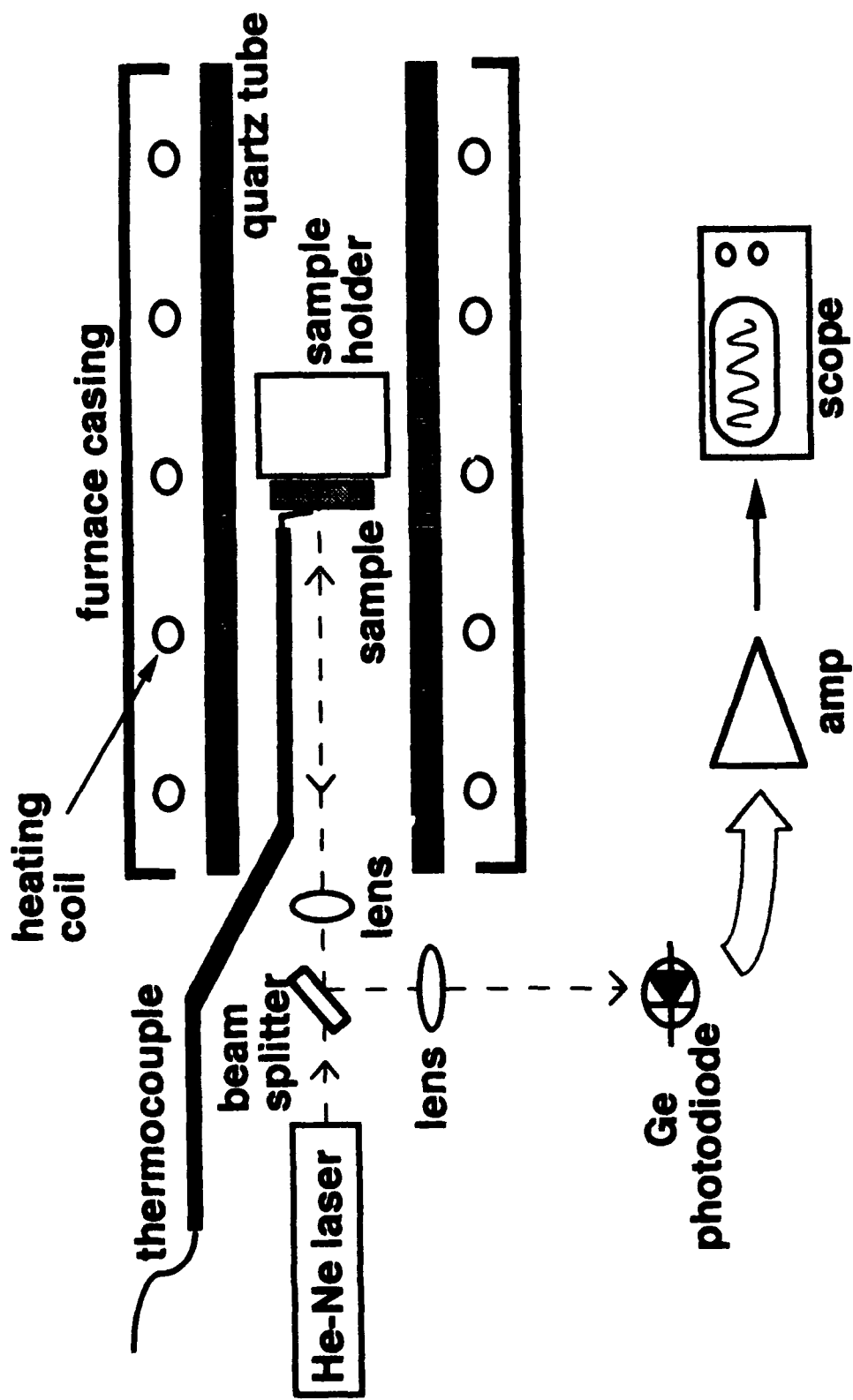


Fig. 2 The infrared laser interferometry setup in the annealing furnace

plotter. A Chromel-Alumel thermocouple (with the reference junction kept at 0°C in a constant-temperature bath recirculator) was attached to the sample surface within 2 mm from the laser spot. The thermocouple was in good thermal contact to the laser irradiated area of the substrate. The thermocouple readout was also compared with the thermometer readout and their difference was within $\pm 0.1^\circ\text{C}$. The heating rate was kept at lower than 10°C per minute in order to get high accuracy.

An interferogram trace is shown in Fig. 3. Notice that the signal level goes through a complete cycle for a temperature increment of approximately 2.8°C . This method is thus capable of detecting a temperature change of $\pm 0.7^\circ\text{C}$. The results of interferometric fringe number (ΔN) versus sample temperature (T_s) in $^\circ\text{C}$ are plotted as shown in Fig. 4. Since both phosphorous and arsenic desorbed from the samples at high temperature, our calibration runs could only reach up to 550°C . For each temperature calibration curve, a third order polynomial was fitted:

$$\text{for GaAs: } T_s = (22.640) + (2.775)\Delta N - (5.8 \times 10^{-4})\Delta N^2 - (4 \times 10^{-6})\Delta N^3,$$

$$\text{for InP: } T_s = (18.692) + (3.024)\Delta N - (4.25 \times 10^{-3})\Delta N^2 + (1 \times 10^{-5})\Delta N^3.$$

The same samples were later mounted on a molybdenum holder and tested in a MBE growth chamber. At each manual power setting, the substrate heater heated the sample up to $T_0 + \Delta T$ (T_0 is the reference temperature, about 22°C) and the interferogram was recorded. After the interferogram had stabilized, a slightly higher heating power was set, and the same detection cycle would repeat. A certain number of oscillations of the reflectance signal corresponds to a certain temperature change ΔT of the substrate. The substrate temperature was determined by adding the temperature change deduced from the reflectance signal to the initial reference temperature T_0 . According to the calibration between the substrate temperature T_s and the fringe number ΔN , obtained in the annealing furnace, the substrate temperature as a function of the substrate heating power (percentage of the total output) could be calibrated, as shown in Fig. 5. Using this method, we found that different molybdenum substrate holders would give a little

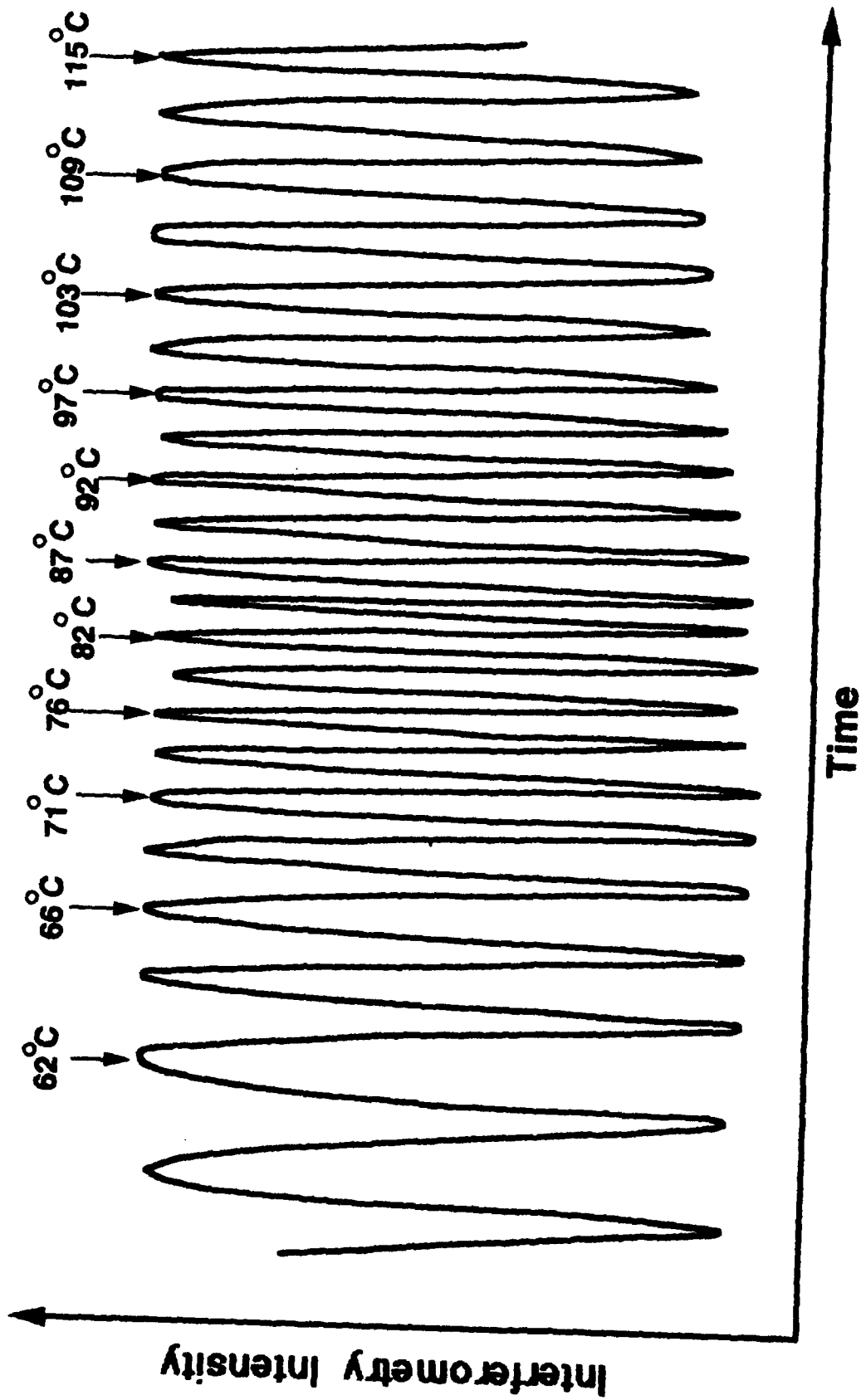


**Fig. 3 Interferogram of 500- μ m-thick GaAs sample by
1.15- μ m He-Ne laser inside a furnace**

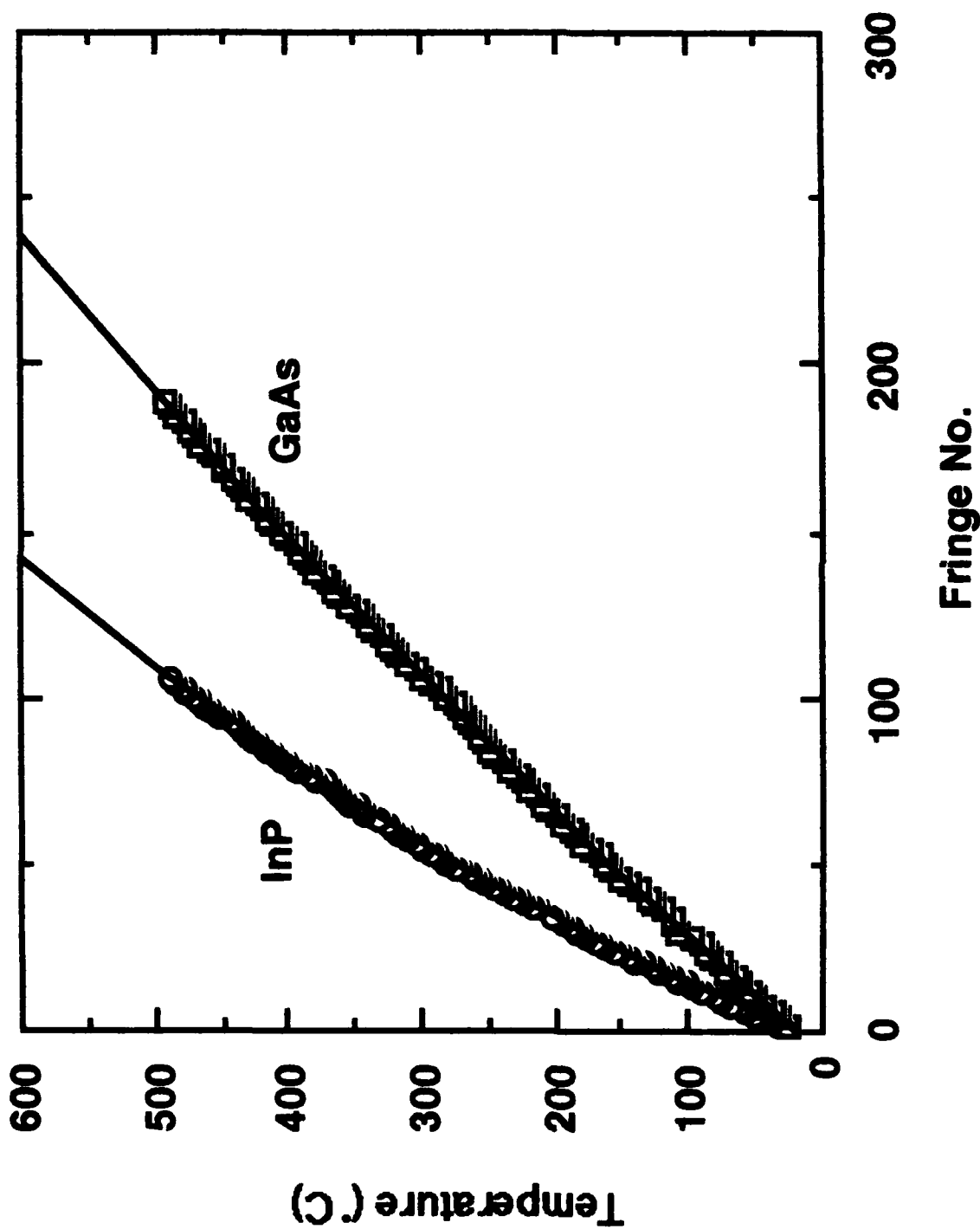


Fig. 4 Temperature Calibration curves for GaAs and InP samples by IR laser interferometry in a furnace

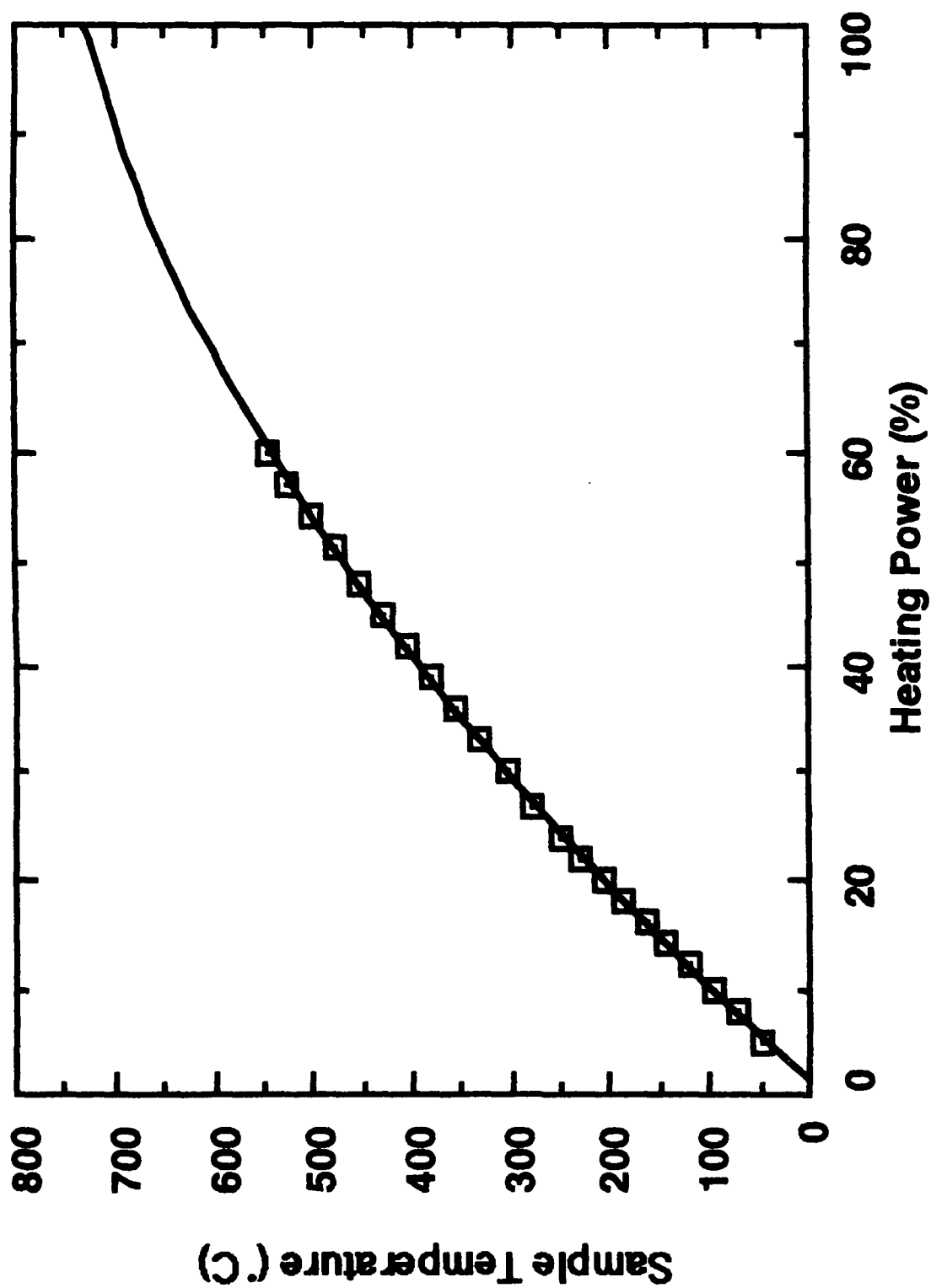


Fig. 5 Substrate heating power vs. sample temperature calibrated in MBE growth chamber

different substrate temperature for the same substrate heater power setting because of different radiation reflectivity. Other growth conditions were also examined using this method.

(1) Without applying any heating power, the introduction of liquid N₂ effectively brought the sample temperature 35°C to 40°C below the room temperature. After the heating power was turned on, the samples could reach the same final temperature but after a longer time.

(2) Because of its relatively low furnace temperature (~300°C), the opening of the arsenic source shutter had almost no effect on the substrate temperature. On the other hand, due to its high furnace temperature (~1000°C), the opening of the Ga source shutter caused a temperature increment of about 10°C on the sample.

2.1.3 Measurement of Ar Ion Laser Induced Local Heating

An Ar⁺ laser (multiline mode) focused to a spot size of 400 μm was irradiated onto a GaAs substrate as shown in Fig. 6. Although the He-Ne laser was incident 5° away from the normal of the sample surface, it merely introduced an error of 0.38 percent which is acceptable. An insulation layer (a double-sided masking tape) was placed between the sample and the sample holder. If an indium solder were used to secure the sample onto the sample holder, a temperature gradient would result across the sample thickness while the Ar⁺ laser was on (since the thermal mass of the sample holder is much greater than that of the sample itself and the sample holder would work as a heat sink). This would destroy the uniformity of the sample refractive index, and hence degrade the interferogram. The insulation layer was to prevent this from happening. Nevertheless, both methods of sample attachment (with In and with an insulation layer) were tried, and the results were analyzed.

The interferograms for Ar⁺ laser induced heating are shown in Fig. 7. The top trace was obtained with an insulating layer positioned between the GaAs sample and the

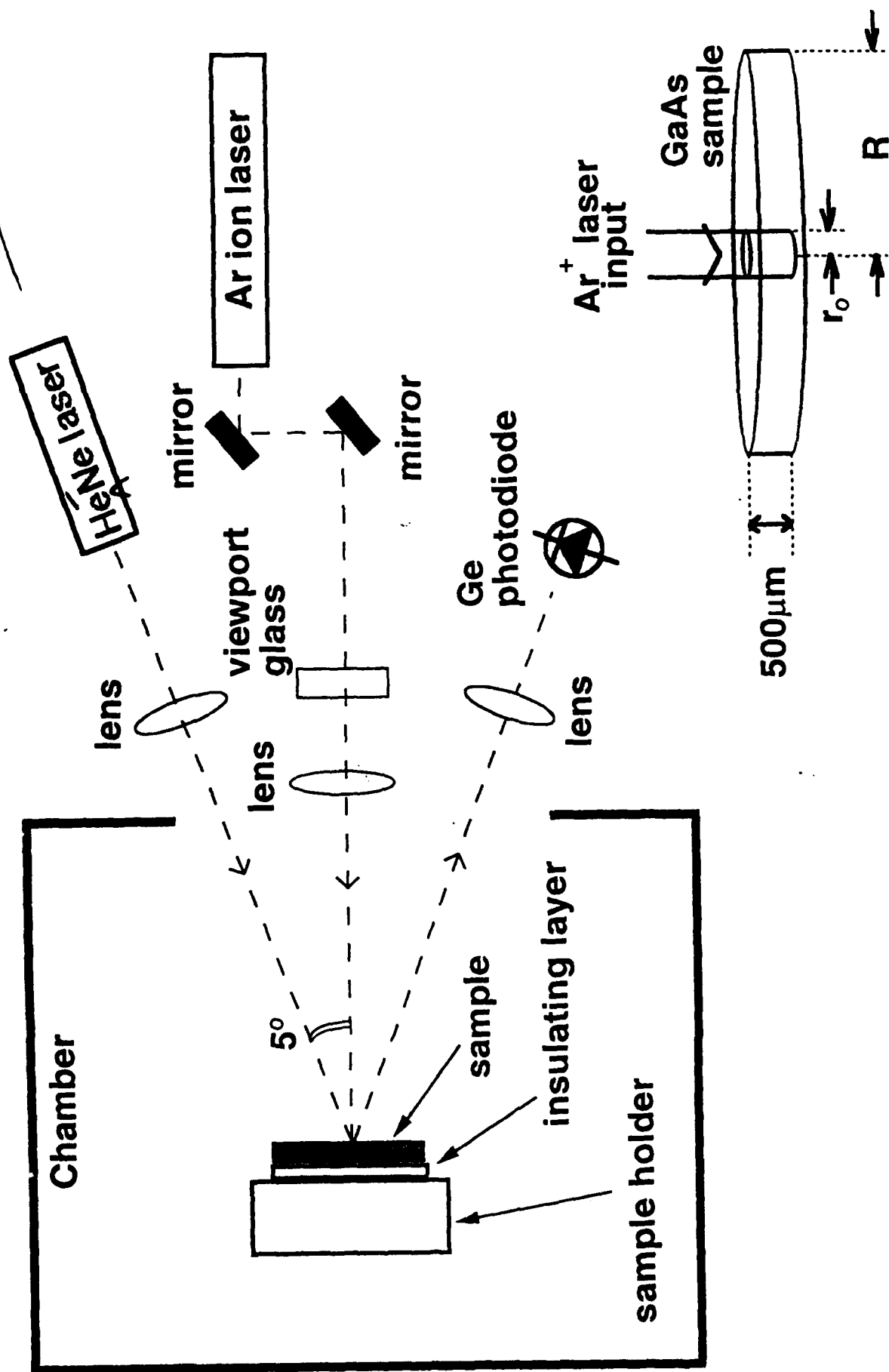


Fig. 6 Measurement setup of substrate temperature change induced by Ar ion laser heating

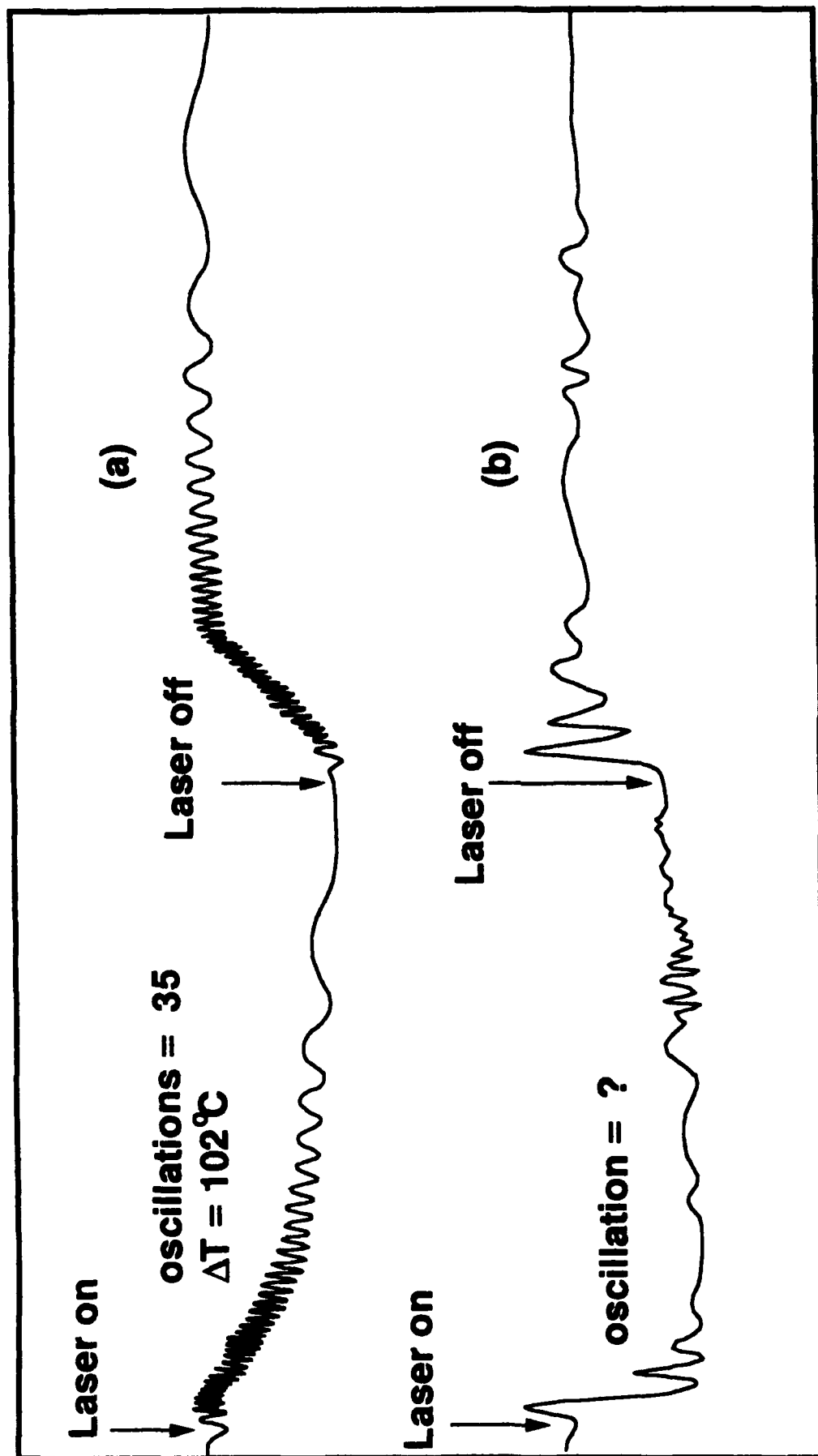


Fig. 7 Interferogram of GaAs sample under 5-W Ar ion laser irradiation
(a) without In attachment: clear oscillations during heating and cooling (b) with In attachment: unclear oscillations

sample holder. The bottom trace was obtained with the GaAs sample thermally attached to the sample holder with indium. It is clear how the indium bonding destroyed the interferogram. Our approximation for the surface temperature of the beam spot was based on the top trace, and the data points of the GaAs beam-spot surface temperature and the corresponding Ar⁺ laser output power are plotted in Fig. 8.

To check whether the experiment made sense or not, a theoretical model was developed (see insert of Fig. 6) and a few verifying numbers were calculated. If we define T(r) as the front surface temperature at a radius r, then in a cylindrical coordinate, the front surface temperature over the edge of the Ar⁺ laser beam spot should be [11]

$$T(r_0) = T(R) + \frac{Q_{\text{center}} \times \ln(R/r_0)}{2 \cdot \pi \cdot l \cdot k}$$

Where r_0 = Ar⁺ laser beam radius = 0.02 cm; R = sample radius = 0.5 cm; l = sample thickness = 0.05 cm; k = GaAs thermal conductivity = 0.4445 watts/cm · °C; and Q_{center} = the amount of heating power being pumped into the center of the GaAs sample from the Ar⁺ laser.

At 5 watts of radiation power from the Ar⁺ laser, the actual thermocouple measurement gave us $T(R) = 106^\circ\text{C}$ (the thermocouple was attached to the sample front surface about 1 mm from the Ar ion laser spot). Furthermore, we found from measurement that the reflectivity of the mirrors is 65.2 percent; the viewport glass transmittance 82.6 percent; the lens transmittance 98.5 percent; and the reflectivity of the polished GaAs front surface 51.5 percent. Thus, only 25.7 percent of Ar⁺ laser power was absorbed in the GaAs sample. Finally, since the absorption coefficient of GaAs at $\lambda = 488$ nm and 514 nm is about $8.9 \times 10^4 \text{ cm}^{-1}$, almost all (about 99.99 percent) of the incident laser energy is absorbed in the 500- μm -thick sample. Thus, for a 5-watt output from the Ar⁺ laser, we estimate $T(r_0)$ to be 137°C . From the IR interferometry method, we found the beam spot temperature to be approximately 124°C , which is in fair agreement with the theoretical value.

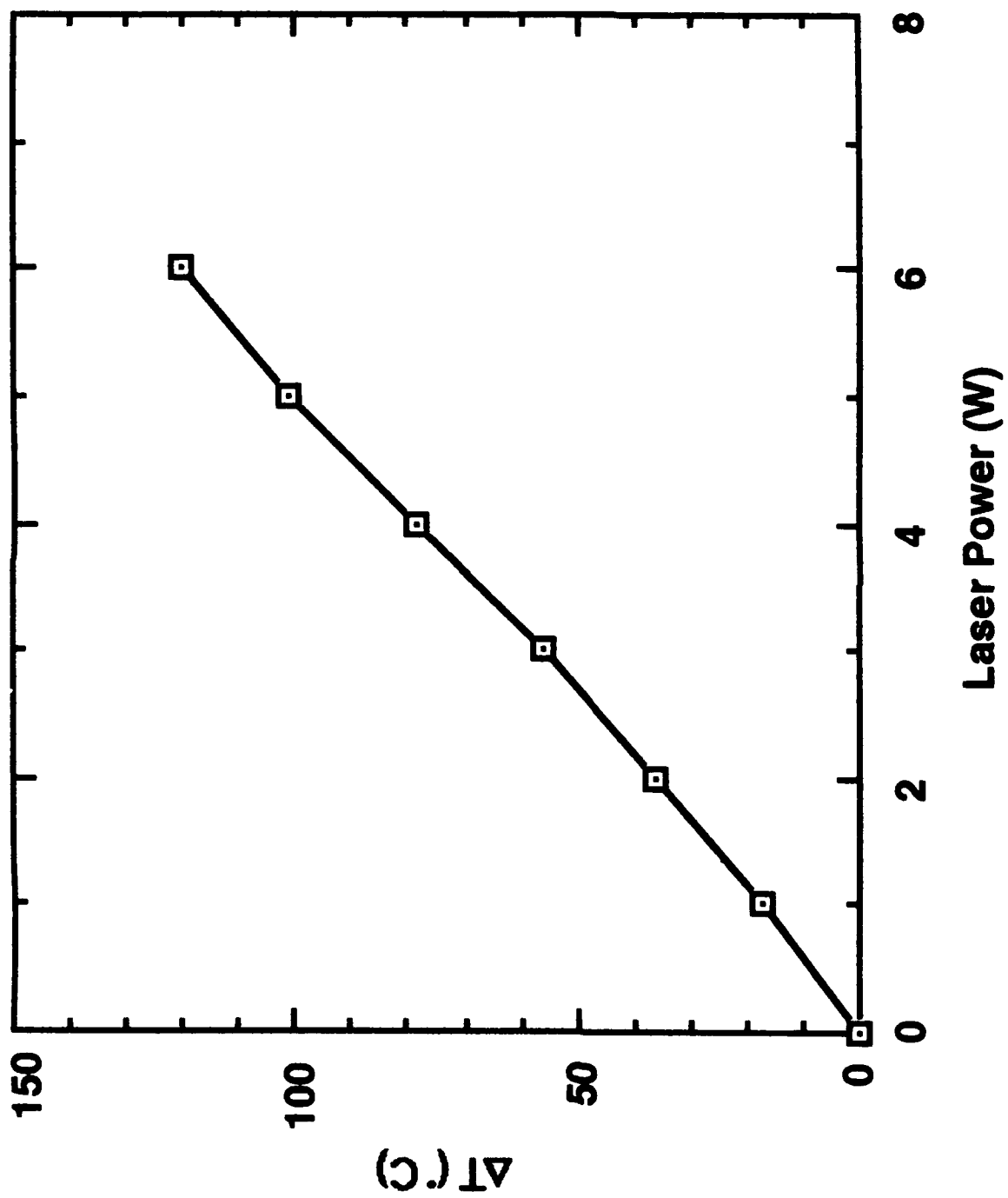


Fig. 8 GaAs sample surface temperature increment versus Ar ion laser power output

2.2 MOMBE Growth

The use of gaseous sources in growing III-V semiconductor compounds in an MBE system has gained increasing interest not only for the fundamental studies of growth kinetics but also for device applications due to its potential of high throughput and selective-area growth and doping. As a method that combines some aspects of MBE and MOCVD, MOMBE/CBE growth is a process more complicated than the conventional MBE growth. Because MOMBE growth takes place in an ultrahigh vacuum chamber, RHEED can be used to clarify the growth mechanisms. In our previous studies on MOMBE, we have proposed a kinetic model that includes both group-III alkyls and arsenic in the surface chemical reactions during MOMBE growth [12,13]. The model can fit the growth-rate data for GaAs and InAs very well and leads to a better understanding of the MOMBE growth mechanism. In order to perform the laser-assisted MOMBE growth, we need to study the MOMBE growth behavior in more detail to obtain enough data for comparison. Here we studied the effects of varying the group-III (TEGa or TMIn) flow rate and group-V (arsenic) flux on the growth rate over a wide range of substrate temperatures. Both the group-III-induced and group-V-induced growth were studied, and it turns out that we need to modify our previous growth model to fit the data.

2.2.1 Growth Study of GaAs and InAs by RHEED

The experimental system will be discussed in Section 2.3.1. Triethylgallium (TEGa) and Trimethylindium (TMIn), which are controlled by MKS model 1150B vapor source mass flow controllers, are injected into the MBE chamber through our home-made gas manifold, and solid arsenic source is used as the group-V material. The RHEED intensity oscillation is used to measure the growth rate. In the growth of III-V compound semiconductors, the V/III flux ratio is a key parameter for the control of materials quality

and composition determination. Although the beam flux ion gauge gives us a value of V/III flux ratio, this value is not the actual V/III incorporation ratio and it varies in different systems. By studying both the group-III and group-V induced RHEED oscillations, we establish a quantitative method of obtaining the actual V/III incorporation ratio.

Fig. 9 shows the GaAs growth rate versus substrate temperature at different TEGa flow rate (0.1-0.35 sccm) for an arsenic flux of 3.0×10^{-6} torr. The data are similar to those from other studies [14,15] except that we did not study the growth for substrate temperatures lower than 400°C. The growth rate stays almost constant in the temperature range of 420-580°C because the pyrolytic decomposition of TEGa is complete above 420°C, but it decreases when the substrate temperature is higher than 580°C which is due to the TEGa desorption at high temperature. When the TEGa flow rate is higher than 0.35 sccm, the relation between the growth rate and the substrate temperature changes greatly.

Fig. 10 shows the growth rate versus TEGa flow rate at different substrate temperatures under an arsenic flux of 3.0×10^{-6} torr. From Fig. 9, we know that GaAs growth rate is independent of the substrate temperature for substrate temperatures in the range of 420°C to 580°C. At low TEGa supply rates, the GaAs growth rate follows a linear relation with respect to the flow rate for all different substrate temperatures, and an arsenic stabilized (2x4) surface reconstruction is observed. This linear relation extends up to about 0.35 sccm TEGa flow rate, where the growth rate reaches its maximum value. Therefore, for TEGa flow rate smaller than 0.35 sccm, the growth is Ga-controlled and the highest growth rate we can achieve is about 1.0 ML/sec for the given arsenic flux. For the low substrate temperature conditions (460°C and 500°C), the growth rate starts to decrease gradually as the TEGa flow rate increases beyond 0.4 sccm, and the RHEED pattern still shows the (2x4) arsenic-stabilized surface reconstruction up to the highest TEGa flow rate used in our experiment (0.6 sccm). At higher TEGa flow

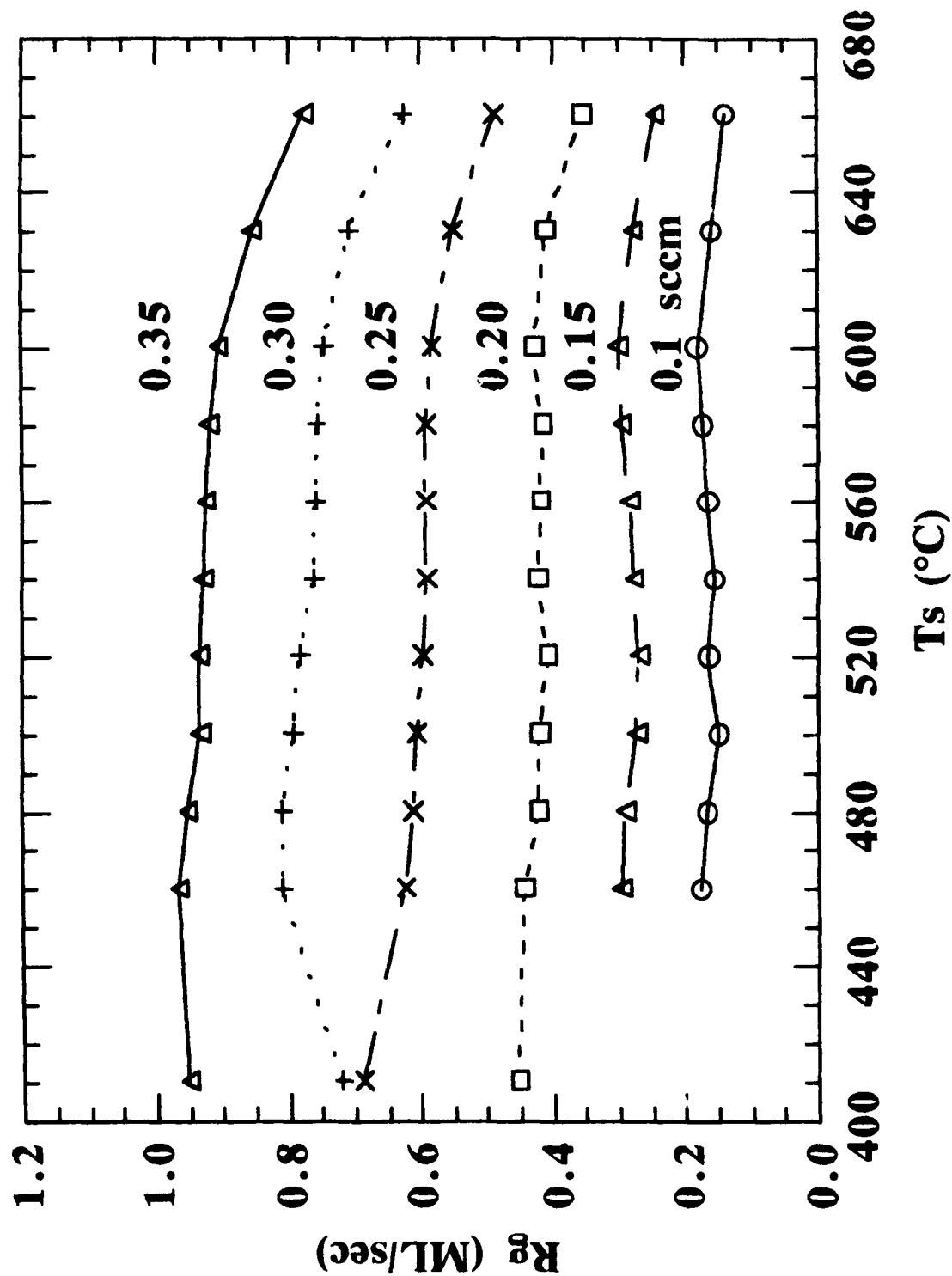


Fig. 9 GaAs growth rate versus substrate temperature at different TEGa flow rate for an arsenic flux of 3.0×10^{-6} torr

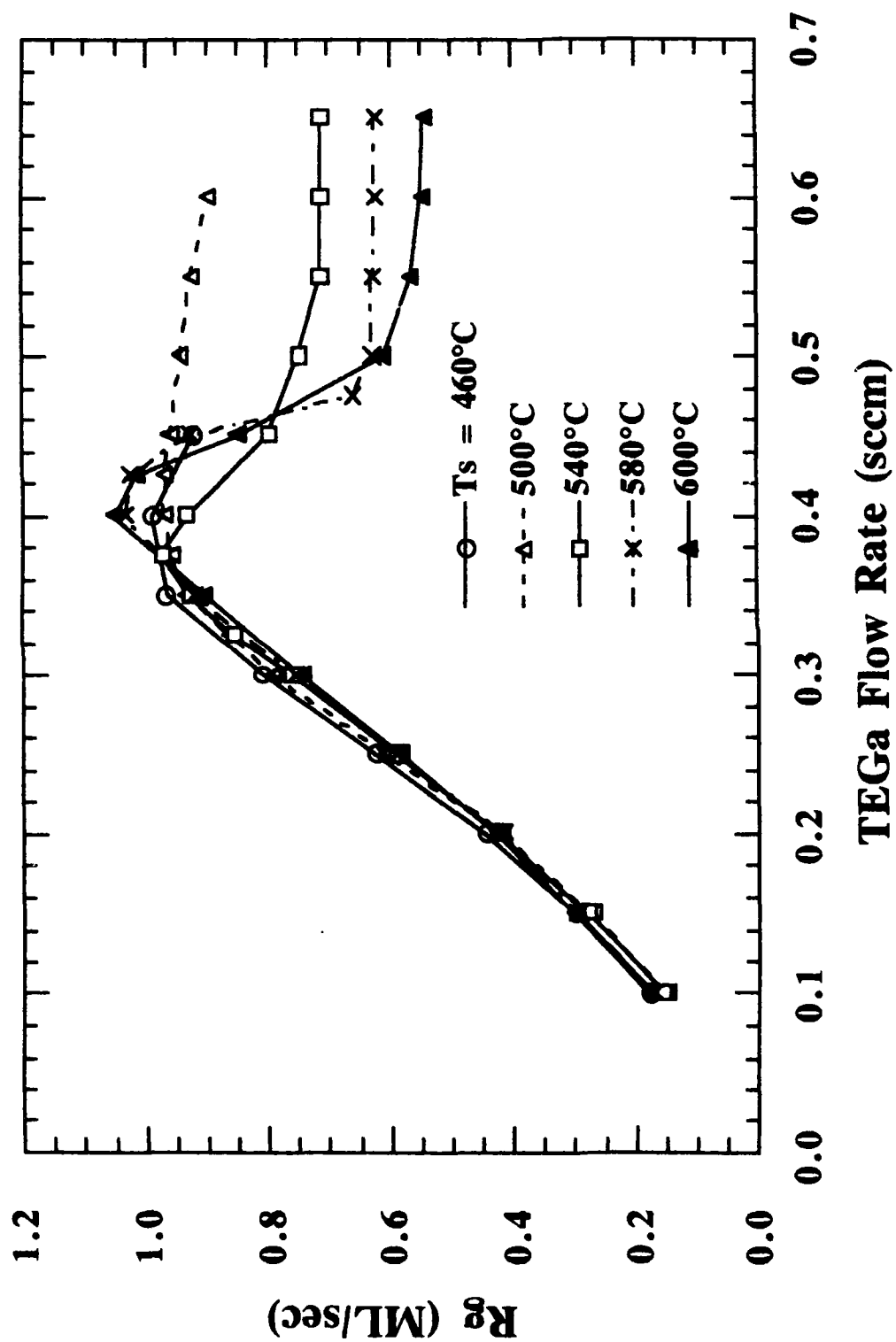


Fig.10 Growth rate versus TEGa flow rate at different substrate temperatures under an arsenic flux of 3.0×10^{-6} torr

rate, the RHEED intensity oscillation is difficult to observe. However, the (2x4) RHEED pattern becomes less and less clear as the TEGa flow rate increases. For the substrate temperature higher than 540°C, the figure clearly shows a transition region where the growth rate decreases as the TEGa flow rate increases past 0.35 sccm, and the growth rate then reaches a stabilization region where it does not change with the TEGa flow rate. In the transition region, the RHEED pattern changes from (2x4) to the Ga-stabilized (4x2) reconstruction. In the stabilization region, the RHEED pattern becomes (4x2) immediately as growth starts. The higher the substrate temperature is, the lower the growth rate will be in the stabilization region. From the figure, we can see that the transition point at substrate temperatures of 580°C and 600°C occurs at a higher TEGa flow rate with a higher growth rate than at the other three lower substrate temperatures. Since the desorption of TEGa takes place when the substrate temperature is higher than 580°C, a higher TEGa flow is needed in order to maintain a unity V/III incorporation ratio and hence the transition point occurs at a higher TEGa flow rate. The shift of transition point to a higher TEGa flow rate extends the linear region and a higher TEGa flow gives a higher growth rate. A similar growth behavior is observed when the arsenic flux is changed to 2.5×10^{-6} torr and 4.0×10^{-6} torr, as shown in Figs. 11 and 12, respectively. We see that the highest growth rate in these two cases is about 0.9 ML/sec and 1.5 ML/sec, respectively. The transition point changes as the arsenic flux changes. The higher the arsenic flux is, the higher the transition point of the TEGa flow rate will be. The shift of transition points at different substrate temperatures is clearly seen in Fig. 12, and the growth rate at the transition point is higher for higher substrate temperature. The growth rate at a substrate temperature of 630°C in the linear region is much lower than those at lower substrate temperatures which is due to the desorption of TEGa.

Typical RHEED intensity oscillation data for the three different regions (linear, transition and stabilization) are shown in Figs. 13 (a), (b), and (c), respectively. The RHEED oscillation data in the gradual-decrease region at low substrate temperature is

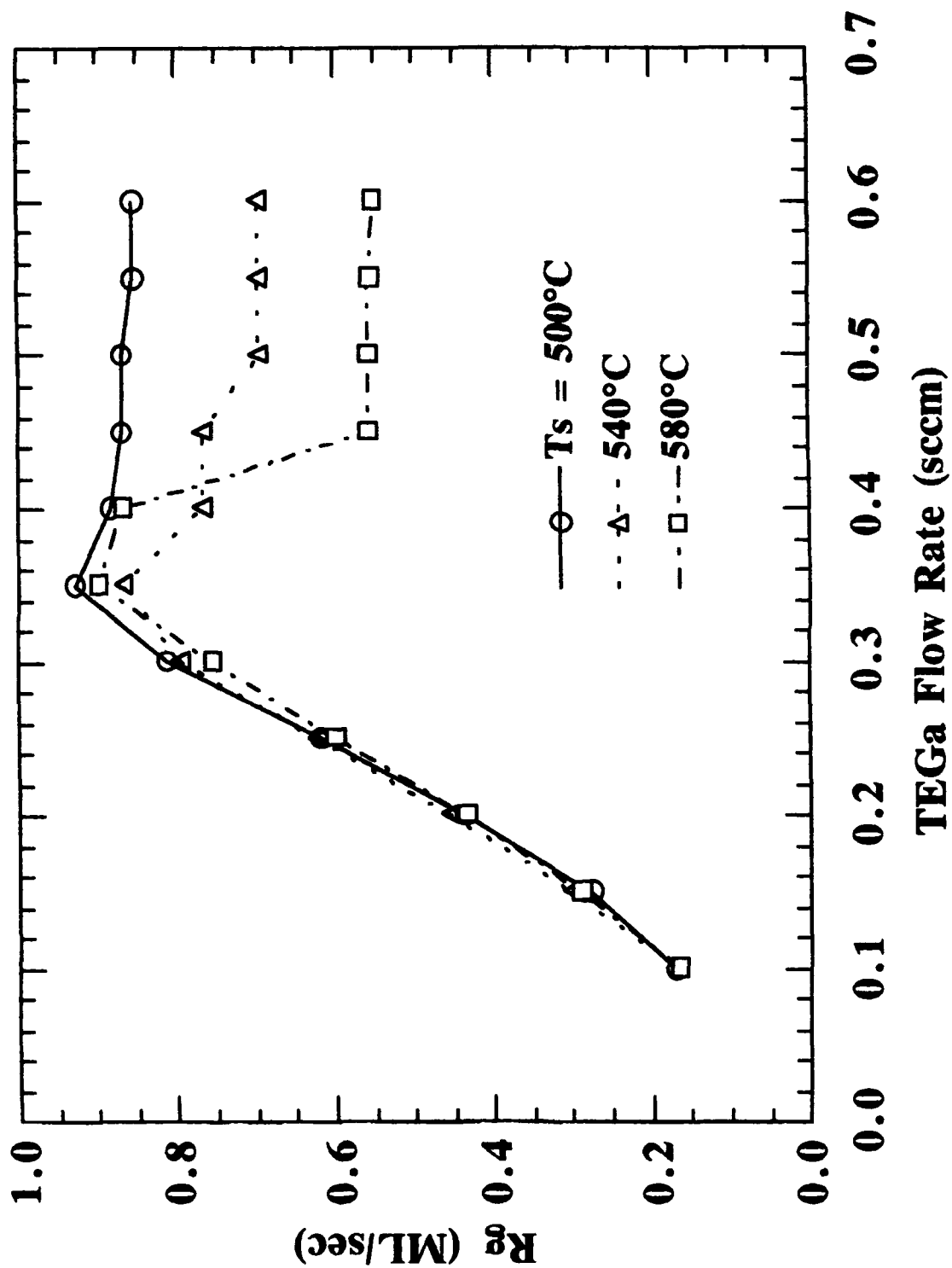
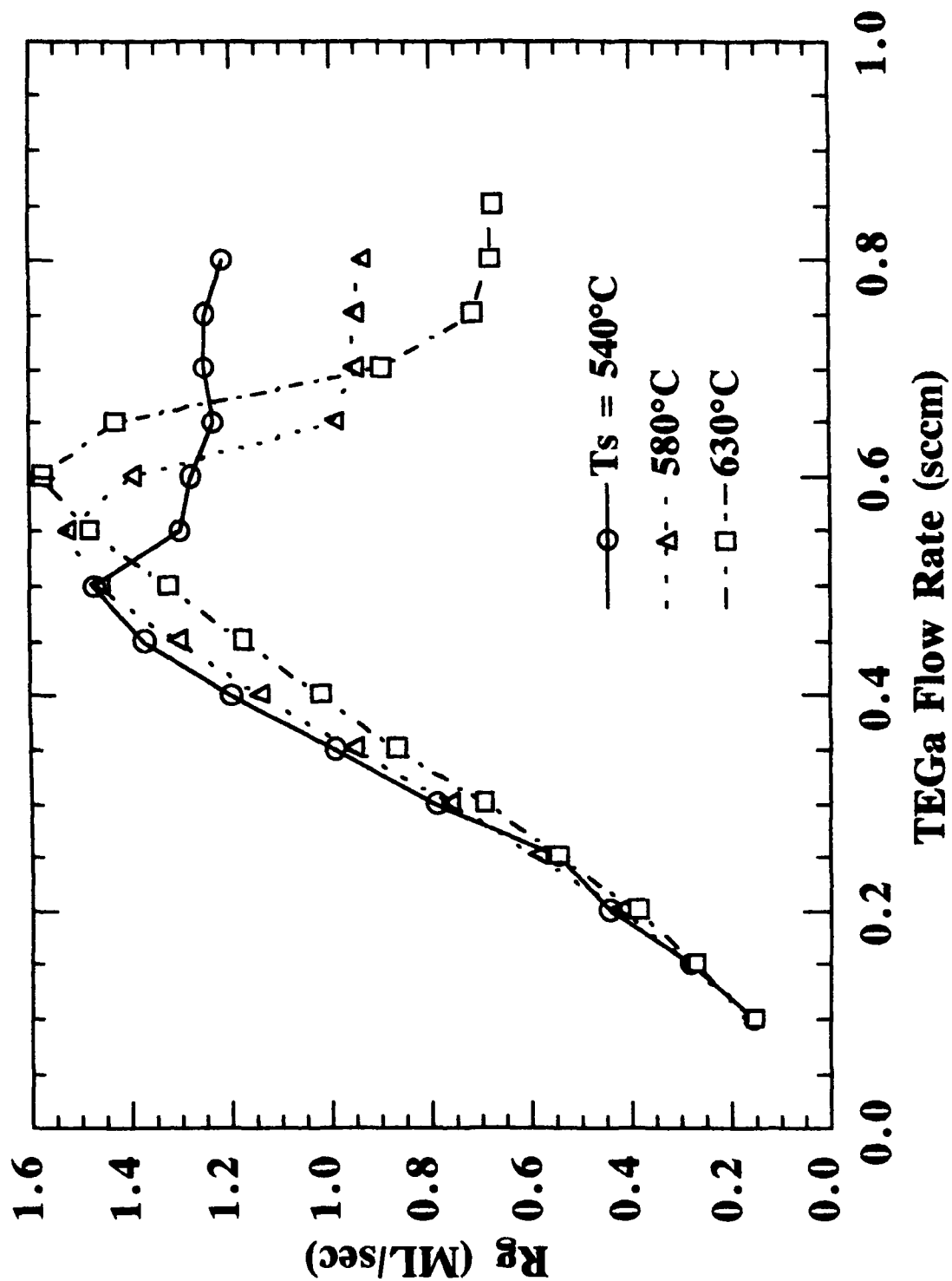


Fig. 11 Growth rate versus TEGa flow rate at different substrate temperatures under an arsenic flux of 2.5×10^{-6} torr



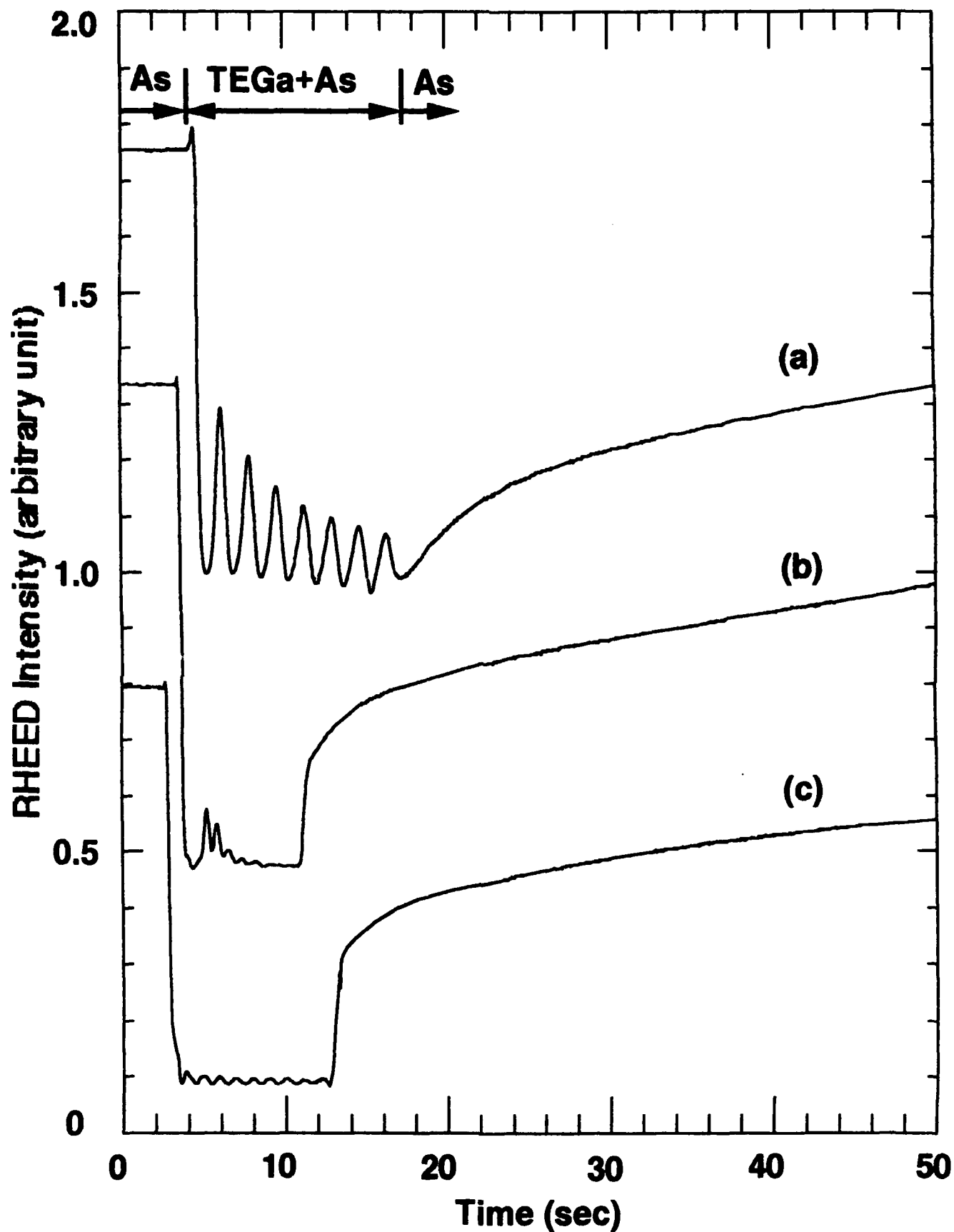


Fig. 13 RHEED intensity oscillation data for (a) linear region, (b) transition region, and (c) stabilization region

similar to the RHEED data in the linear region at high substrate temperature. We see clearly from Fig. 13 that the RHEED oscillation amplitude in the linear region is much larger than that in the stabilization region. From our knowledge of RHEED intensity oscillation, we know that the growth is controlled by Ga incorporation (with larger amplitude) in the linear region and is controlled by As incorporation (with smaller amplitude) in the stabilization region. In the transition region, Ga-controlled incorporation and As-controlled incorporation compete with each other at first, but the growth will become As-controlled eventually. The RHEED oscillation number in the transition region is far less than the other two regions due to this competition, and the amplitude is larger (similar to that in the linear region) at first and becomes very small after several layers of growth (similar to that in the stabilization region). The decrease of the growth rate when the substrate temperature is increased in the stabilization region is proposed to be due to arsenic desorption. The stabilization happens when the substrate temperature is above the arsenic desorption temperature (about 520°C), and the arsenic surface concentration becomes lower as the substrate temperature increases. In the arsenic-controlled growth process, the growth rate is lower as the arsenic surface concentration is lower.

We have also studied the arsenic-induced growth by the RHEED intensity oscillation technique. Fig. 14 illustrates a typical RHEED oscillation and shutter operation sequence during the growth of GaAs at 520°C. It starts with an arsenic-stabilized surface, and the Ga-induced oscillation is observed after the TEGa is introduced. The RHEED intensity decreases after the arsenic shutter is closed due to the Ga accumulation on the substrate, which forms a rough surface. Then the TEGa valve is closed, and the arsenic shutter is opened again. The oscillation resumes with incoming arsenic species reacting with the Ga accumulation on the surface. This represents arsenic-controlled growth because there is an excess amount of Ga adatoms on the surface and the available amount of arsenic

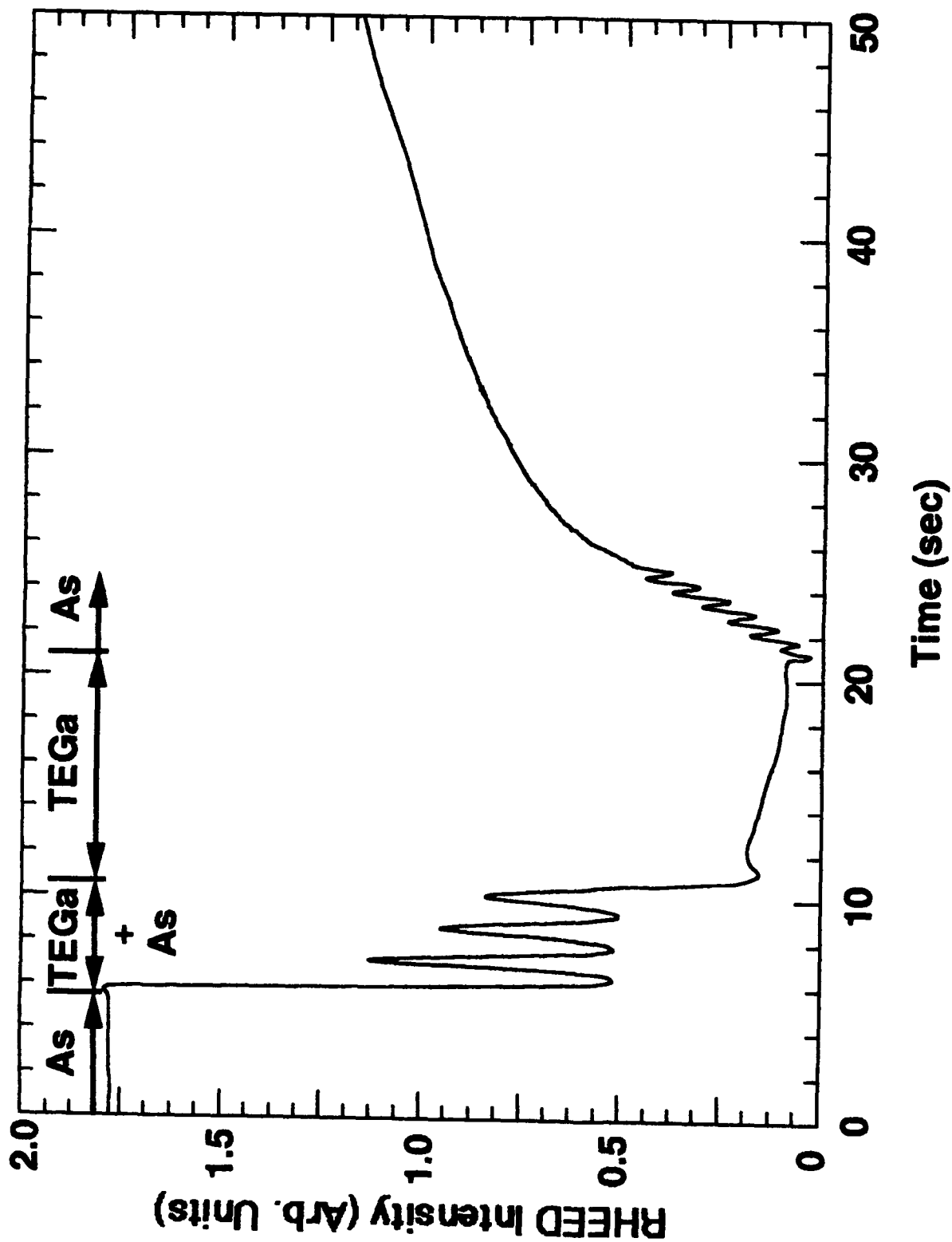


Fig. 14 RHEED oscillations for MOMBE of GaAs using TEGa and arsenic. Both group-III and group-V induced oscillations are shown.

limits the growth rate. Fig. 15 shows the arsenic-induced growth rate as a function of the substrate temperature at a TEGa flow rate of 0.35 sccm for different arsenic fluxes.

The arsenic incorporation rate is constant for low substrate temperatures and starts to decrease, due to arsenic desorption, when the substrate temperature is above 520°C. The arsenic incorporation rate is about 1ML/sec when the arsenic flux is 3.0×10^{-6} torr. Compared to Fig. 10, the Ga incorporation rate is about 1ML/sec at the same arsenic flux and TEGa flow rate (0.35 sccm). In Fig. 12 the Ga-induced growth rate is about 1.5ML/sec at the transition point with an arsenic flux of 4.0×10^{-6} torr at a substrate temperature of 540°C, and the As-induced growth rate is about 1.5ML/sec at the same flux in Fig. 15. Therefore, we conclude that the V/III incorporation ratio is about unity at the transition point. When the V/III ratio is greater than unity, the growth is Ga-controlled, and when the V/III ratio is less than unity the growth becomes very complicated. The growth is still Ga-controlled up to a V/III ratio of 0.5 when the substrate temperature is lower than the arsenic desorption temperature. However, when the substrate temperature is higher than the arsenic desorption temperature, the growth is in the transition region when the V/III ratio is between 0.7 and 1, and in the stabilization region when the V/III ratio is lower than 0.7.

The MOMBE growth behavior of InAs was also investigated using TMIn and solid arsenic by RHEED. Fig. 16 shows the InAs growth rate as a function of TMIn flow rate at two different substrate temperatures (450°C and 460°C) for an arsenic flux of 2.5×10^{-6} torr. There is a linear region and a gradual decrease region, similar to the low-substrate-temperature case for GaAs. The transition and stabilization regions were not observed due to the difficulty of obtaining RHEED intensity oscillations for high TMIn flow rates at high substrate temperatures. Fig. 17 shows the InAs growth rate as a function of substrate temperature for different TMIn flow rate at an arsenic flux of 2.5×10^{-6} torr. The growth rate is almost constant in the substrate temperature range studied at low

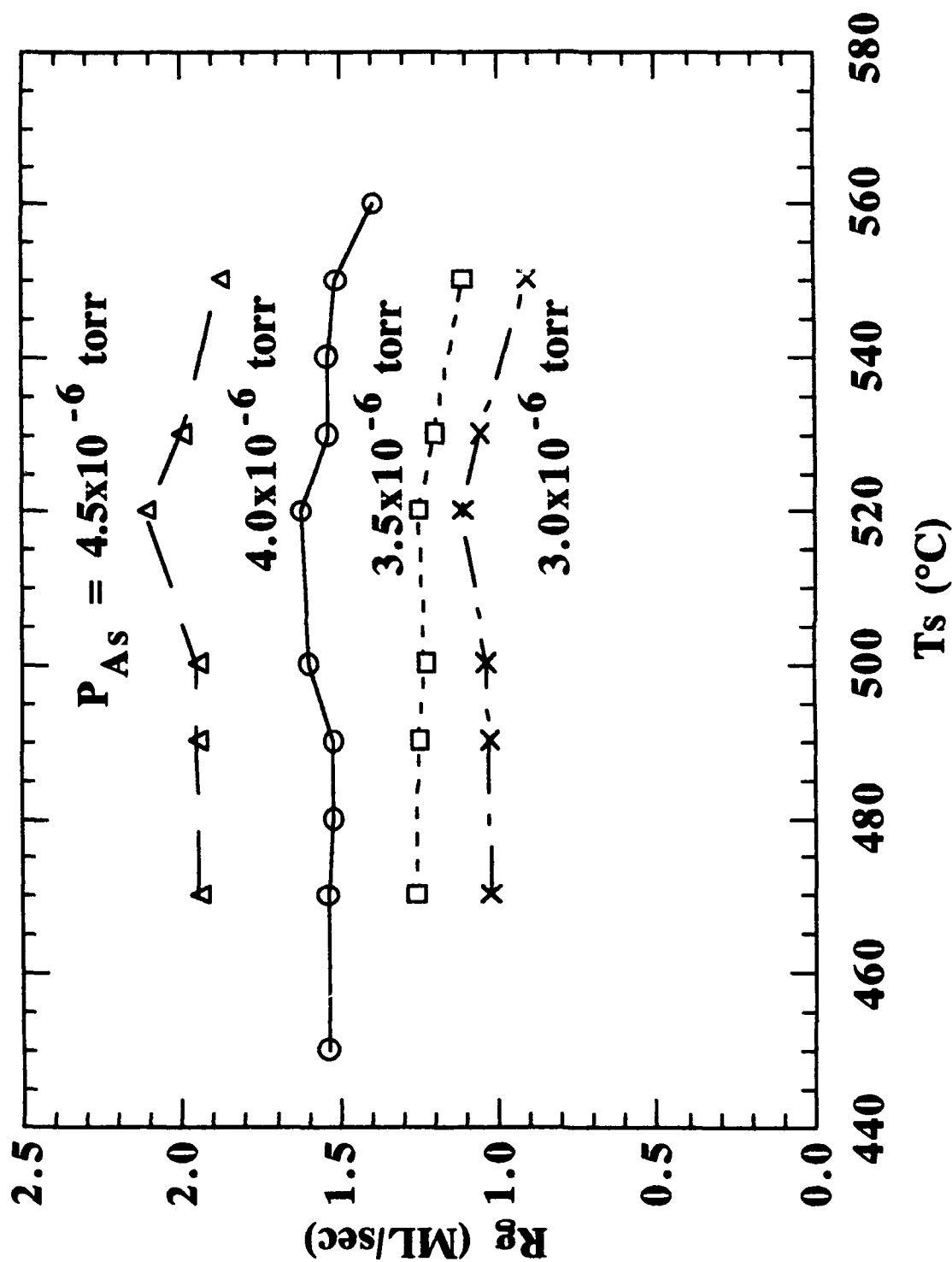


Fig. 15 Arsenic-induced growth rate as a function of the substrate temperature at a TEGa flow of 0.35 sccm for different arsenic fluxes

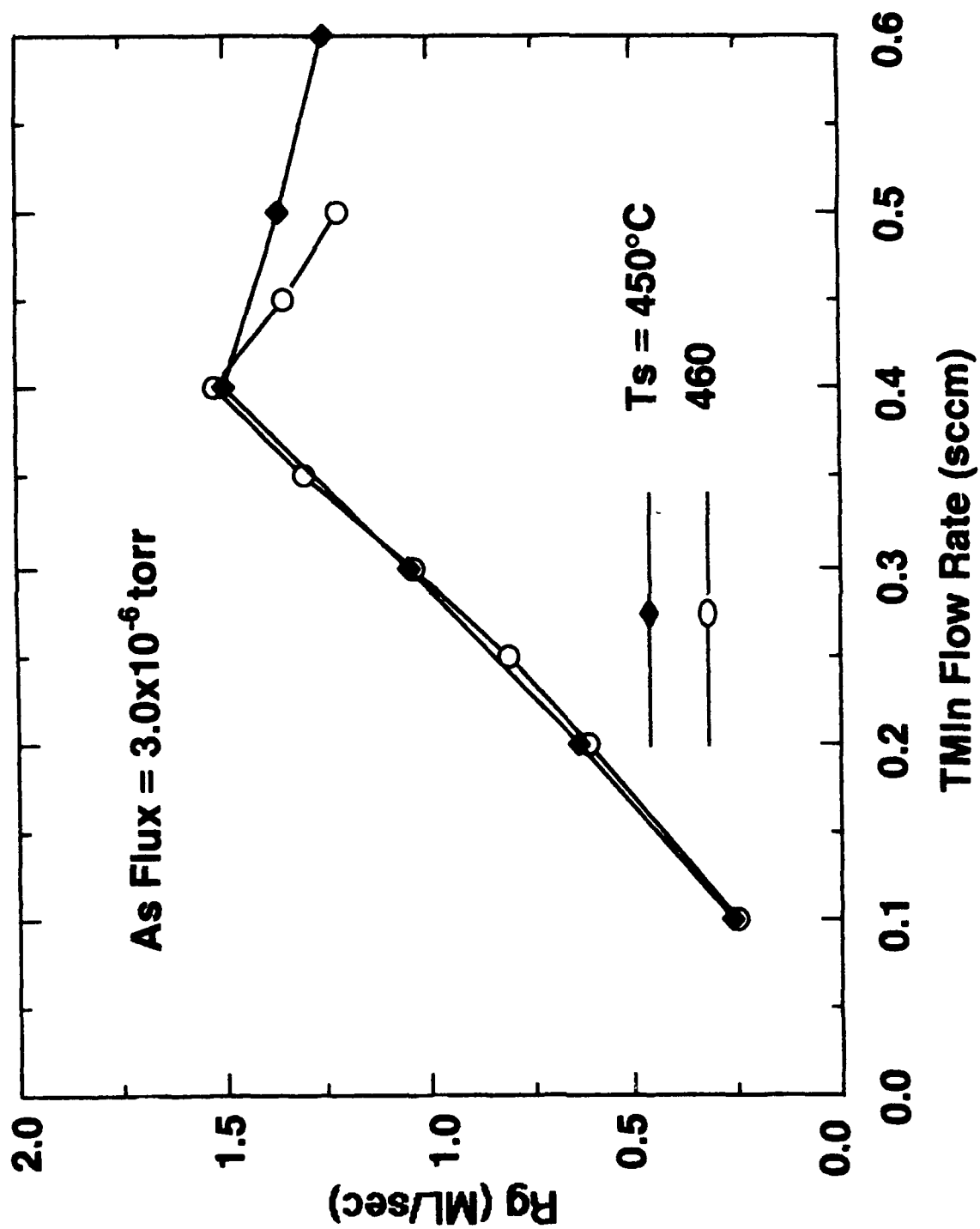


Fig. 16 InAs growth rate as a function of TMIn flow rate

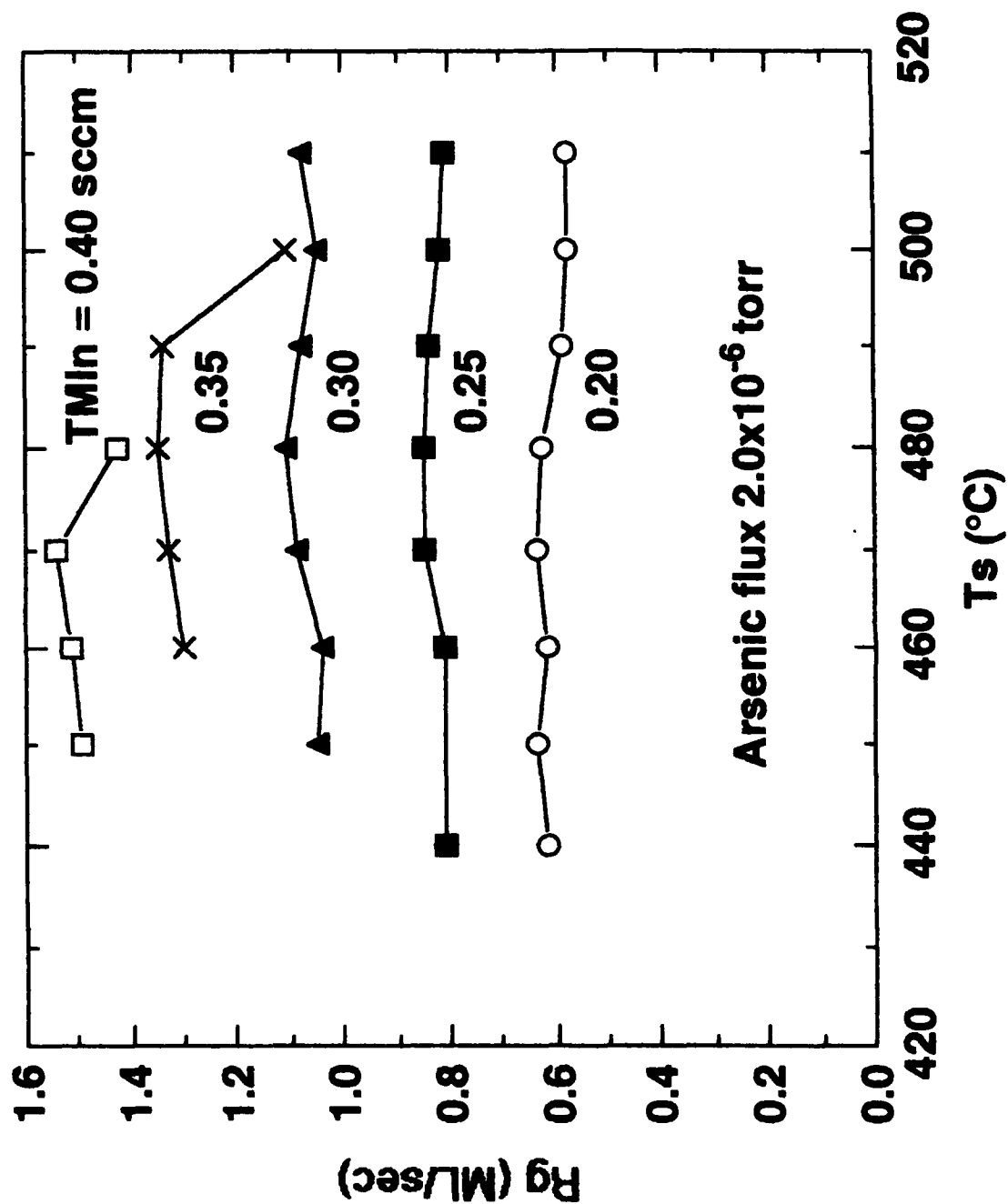


Fig. 17 InAs growth rate as a function of substrate temperature

TMIn flow, while the growth rate decreases at high substrate temperature end when the TMIn flow is high because of the effect of TMIn desorption.

From the above study, we see that our previous growth model only applies in the linear region. In order to better interpret the growth process, we need to use a variable sticking coefficient and different decomposition coefficients for TEGa decomposed on As surface and Ga surface. This will be very complicated and the model is not complete yet.

2.2.2 Characterization of Epitaxial GaAs Layer

So far we have concentrated on understanding the MOMBE growth kinetics. We have not tried to optimize the material quality because in the near future we shall concentrate on CBE growth using alternative group V sources, such as tris-dimethyl amino arsine (TDMAs) and tertiary butyl phosphine (TBP). The epitaxial GaAs layer was characterized by various measurement. Fig. 18 shows the low temperature photoluminescence spectrum of a GaAs sample grown by MOMBE described in the last section. The peaks at 8534 Å and 8734 Å may be related to the metalorganics. The room temperature Hall measurement shows $300 \text{ cm}^2\text{V}^{-1}\text{s}^{-1}$ mobility and $1 \times 10^{17} \text{ cm}^{-2}$ hole concentration.

2.2.3 InGaAs Growth

FitzGerald *et al.* [16] have done the surface chemical studies of the influence of In and Al on the decomposition of TEGa on GaAs (100) substrate. Their simulations show that the presence of Al enhances the Ga deposition rate while the presence of In suppresses the Ga deposition rate. Iimura *et al.* [17] studied RHEED intensity oscillations during the growth of GaAs and InGaAs. They found that the InGaAs growth rate is lower than that of GaAs after the growth of several monolayers of InGaAs and the growth rate is lower for higher substrate temperature. Kobayashi *et al.* [18] studied the

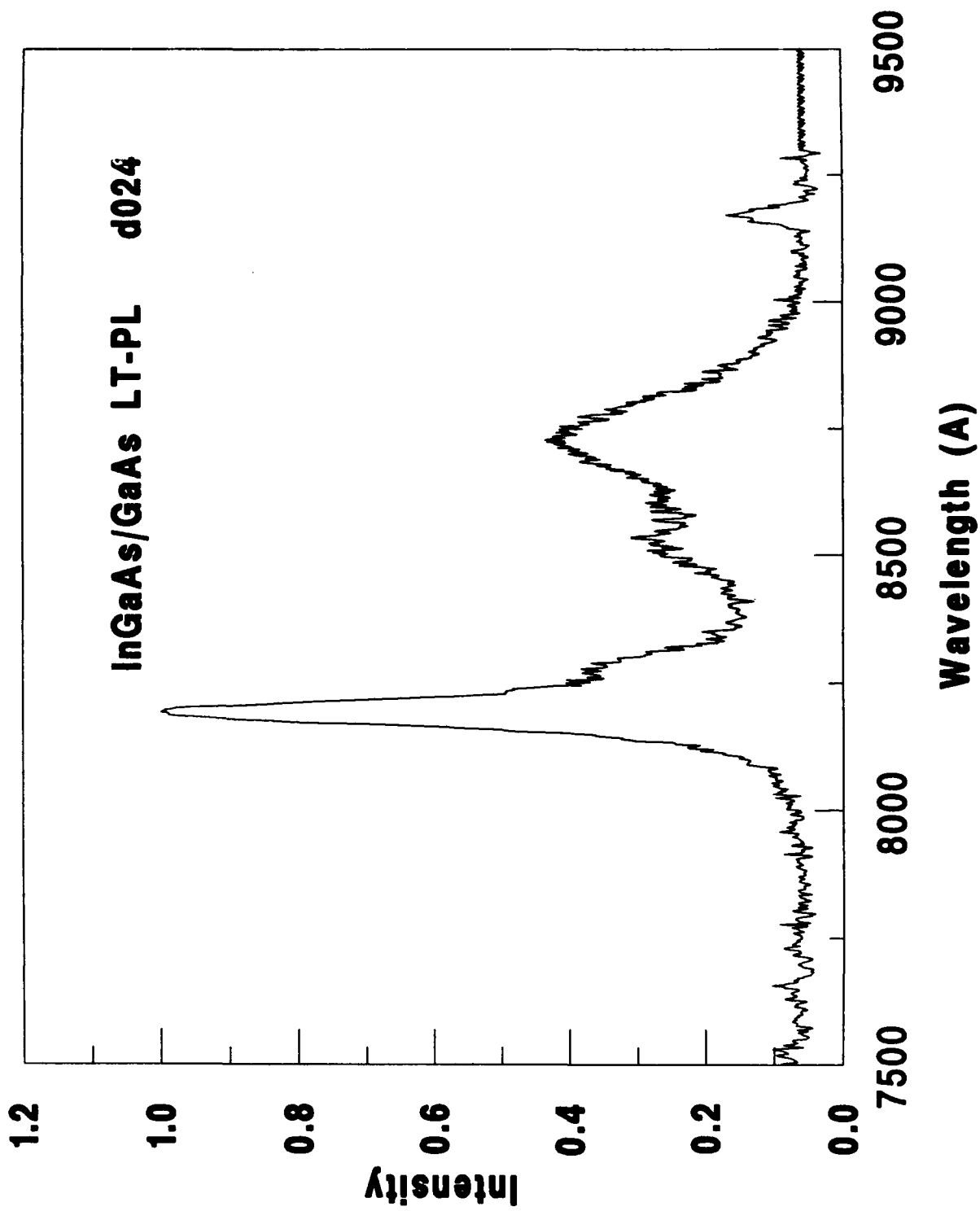


Fig. 18 Low Temperature (8K) photoluminescence measurement for GaAs epilayer

substrate temperature dependence of InGaAs growth rate and four distinct T_s dependent regions were observed.

We also found the same behavior as Iimura *et al.* and the stabilized growth rate becomes lower as the TMIn flow rate increases, as shown in Fig. 19. This is in correspondence to the simulations of FitzGerald *et al.* Surface segregation of indium during growth is proposed to be the reason that InGaAs growth rate becomes lower than that of GaAs. However, the physics is still not clear yet, and we will collect more data on the growth of InGaAs so as to get a control over the ternary growth.

2.3 Ar Ion Laser-Assisted MOMBE Growth

Recently, laser-assisted crystal growth of III-V compound semiconductors has attracted much attention because of its great potential for selective-area growth and doping, and possible application to optoelectronic devices [19]. Both excimer laser and Ar^+ laser have been employed during MOMBE and MOCVD [21-29]. An InGaAsP/InP double wavelength laser has been fabricated successfully by laser-assisted CBE [20]. The growth behavior of various binary and ternary compounds, such as GaAs, InP, GaP, InGaAs, and GaAsP, have been studied, and so far, three models have been proposed for the mechanism of photo-assisted epitaxy: catalytic (or electronic), pyrolytic, and photolytic decomposition of metalorganic molecules. Donnelly *et al.* [21] explained their results with excimer laser irradiation using the pyrolytic decomposition model. In Ar^+ laser-assisted chemical beam epitaxy (CBE) where AsH_3 was used, the heating effect is minor and Aoyagi *et al.* [22] proposed a catalytic process since the growth rate enhancement depends on substrate conductivity. Similarly for Ar^+ laser-assisted CBE of GaAs and GaP, Sugiura *et al.* [25] concluded that the mechanism involved is most likely a photolytic decomposition of the metalorganic molecules since enhanced growth on GaP, which is transparent to the Ar^+ laser beam, exhibits the same behavior as on GaAs.

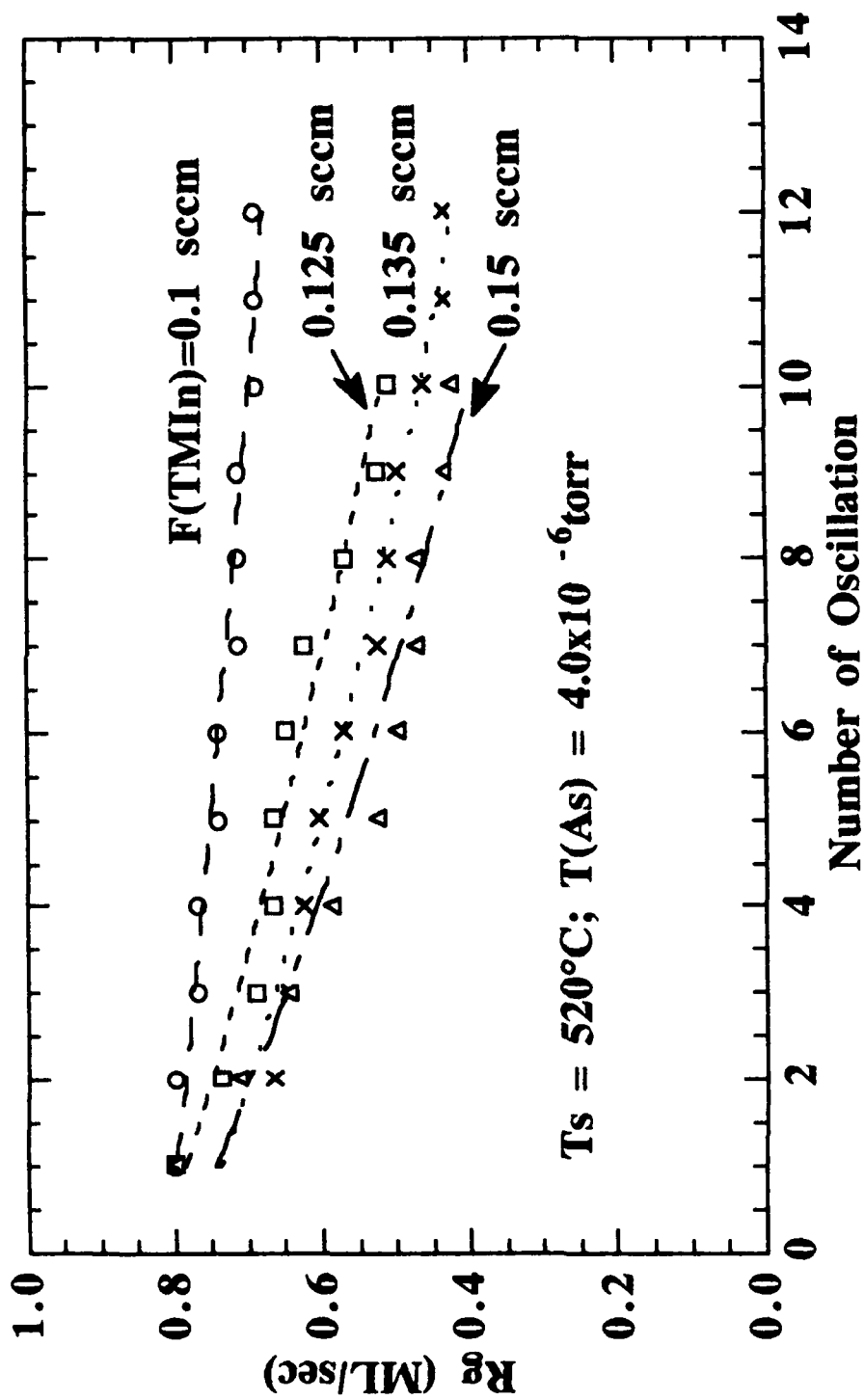


Fig. 19 Transient behavior of InGaAs growth rate. The decrease of growth rate is observed at higher TMIn flow rate

With Ar^+ laser irradiation, the decomposition rate of TEGa on the As plane is enhanced very much in comparison to that on the Ga plane [23], and the epitaxial GaAs layer shows lower carbon incorporation and better optical property [27]. In our work, we investigate the growth behavior with different substrate temperature, arsenic flux and laser power by observing the specular-beam RHEED intensity oscillation. The importance of the arsenic species during the LAMOMBE growth is pointed out.

2.3.1 Laser-Enhanced Decomposition of TEGa

In our LAMOMBE study of GaAs, TEGa molecules, which were introduced into the growth chamber without any carrier gas, and solid arsenic (As_4) were used as source materials. Semi-insulating (001) GaAs substrates were chemically etched and thermally cleaned at about 600°C , and the substrate temperature was calibrated by using the infrared-laser interferometric technique discussed in Section 2.1. An Ar^+ laser (multiline mode) was focused to a $400\text{-}\mu\text{m}$ spot and directed at the substrate at normal incidence. The 10-KeV RHEED electron beam was aligned to the same spot irradiated by the laser beam by adjusting the x-y deflections of the RHEED gun.

We have used RHEED oscillations to study the behavior of Ar^+ laser-assisted GaAs growth in the substrate temperature range of 330°C - 450°C with the laser turned on and off, and the results are shown in Table 1. At temperatures in the range 340 - 420°C , the enhancement of TEGa decomposition with laser irradiation compared to that without laser irradiation is observed. When the substrate temperature is lower than 370°C , there is only laser-assisted growth. There is no laser-assisted growth for substrate temperature lower than 340°C , and there is no change of growth rate for substrate temperature higher than 420°C with or without laser irradiation. The substrate temperature rise is calculated to be about 20°C at $T_s=400^\circ\text{C}$ for a 1-W Ar ion laser with a $400\text{-}\mu\text{m}$ beam diameter, with the model proposed by Nissim *et al.* [30]. Therefore, the pyrolytic decomposition of TEGa alone is not likely. However if photolytic decomposition of TEGa is the only

Table 1 The growth behavior of Ar ion laser-assisted GaAs growth in the substrate temperature range of 330°C-450°C

Substrate temperature (°C)	<340	340-370	370-420	>420
Growth behavior	No growth	Only laser-assisted growth	Enhanced laser-assisted growth	No Enhancement

process, we should be able to obtain GaAs growth with laser irradiation even at a substrate temperature lower than 340°C. Therefore, both pyrolytic and photolytic decomposition of TEGa play roles in Ar⁺ laser-assisted MOMBE growth of GaAs. Here the catalytic effect which depends on the surface electronic status of the substrates was neglected because only semi-insulating GaAs substrates were used in our experiment.

Fig. 20 shows RHEED oscillations with and without Ar⁺ laser irradiation with TEGa and As₄ supply at a substrate temperature of 365°C. After a 2000 Å GaAs buffer layer using solid Ga and As₄ at 580°C was grown, the substrate was cooled down to 365 °C with the Ga shutter closed and the arsenic flux lowered (by closing one of the two arsenic cells in the system). When the temperature was stabilized, TEGa was introduced into the growth chamber. The upper curve in Fig. 20, obtained under Ar⁺ laser irradiation, is totally different from the lower curve with no laser irradiation. The results clearly show that there is GaAs growth with laser irradiation while there is no growth at all without laser irradiation. This RHEED result is verified by a Dektak stylus profiler and Nomarski microscope study.

Fig. 21 shows the RHEED intensity oscillation pattern with and without Ar⁺ laser irradiation with TEGa and As₄ supply at a substrate temperature of 410°C. After the GaAs buffer layer was grown at 580°C and the substrate temperature was cooled down and stabilized at 410°C, TEGa was introduced into the growth chamber and the Ar⁺ laser was turned on at the same time. After seven layers were grown, the Ar⁺ laser was turned off. The oscillations with laser irradiation have much higher amplitudes and slower damping than those without laser irradiation, which indicates the enhancement of the surface migration of TEGa molecules and/or Ga adatoms on the surface with laser irradiation. The growth rate under laser irradiation is a little larger than that without laser irradiation, showing the enhancement of TEGa decomposition under laser irradiation. On the other hand, the enhanced desorption of arsenic with laser irradiation could also have removed the site-blocking effect and increased the growth rate. The

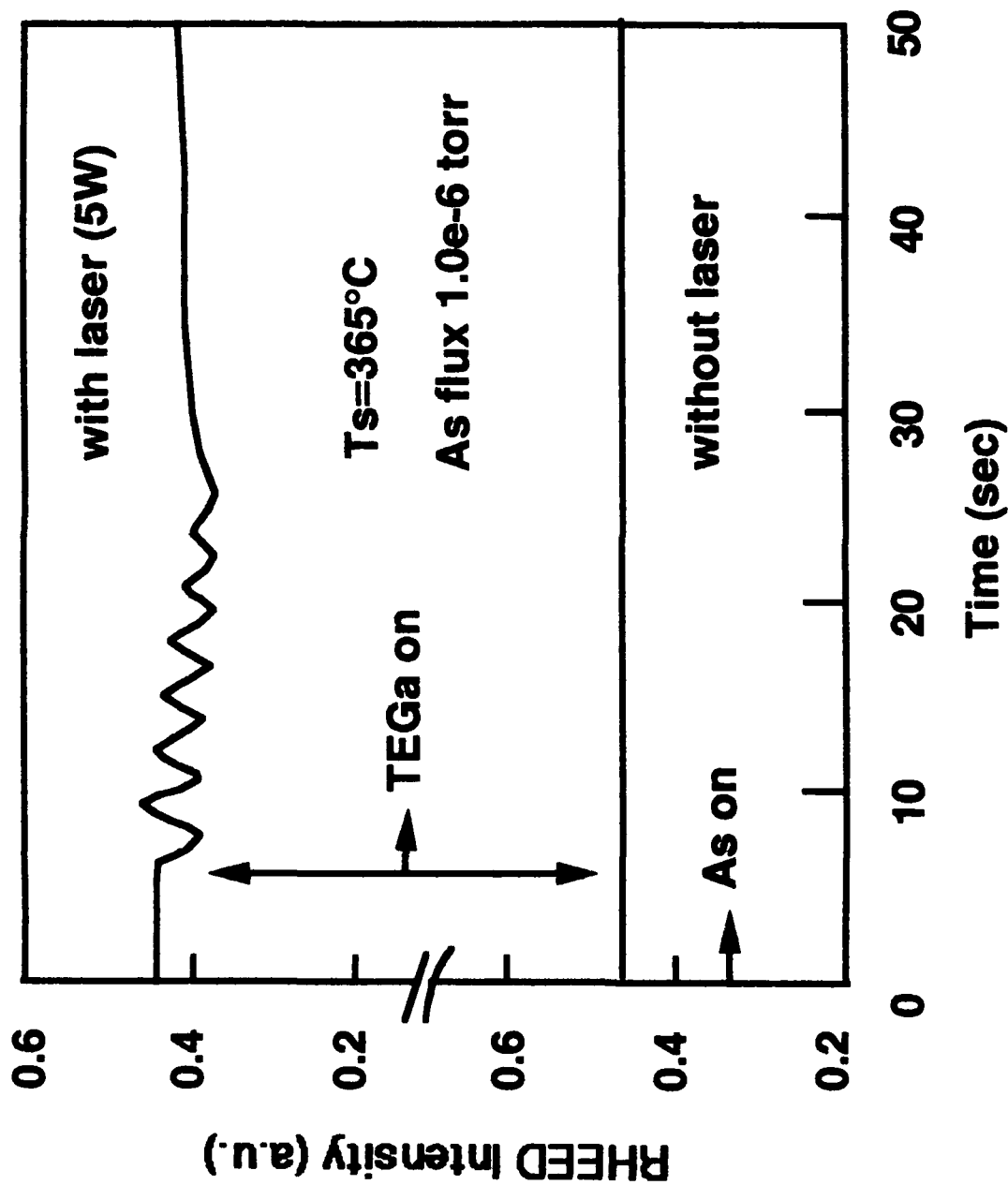


Fig. 20 RHEED oscillations with and without laser irradiation at a substrate temperature of 365°C . Enhanced growth of GaAs is observed with laser irradiation while no growth is without laser irradiation.

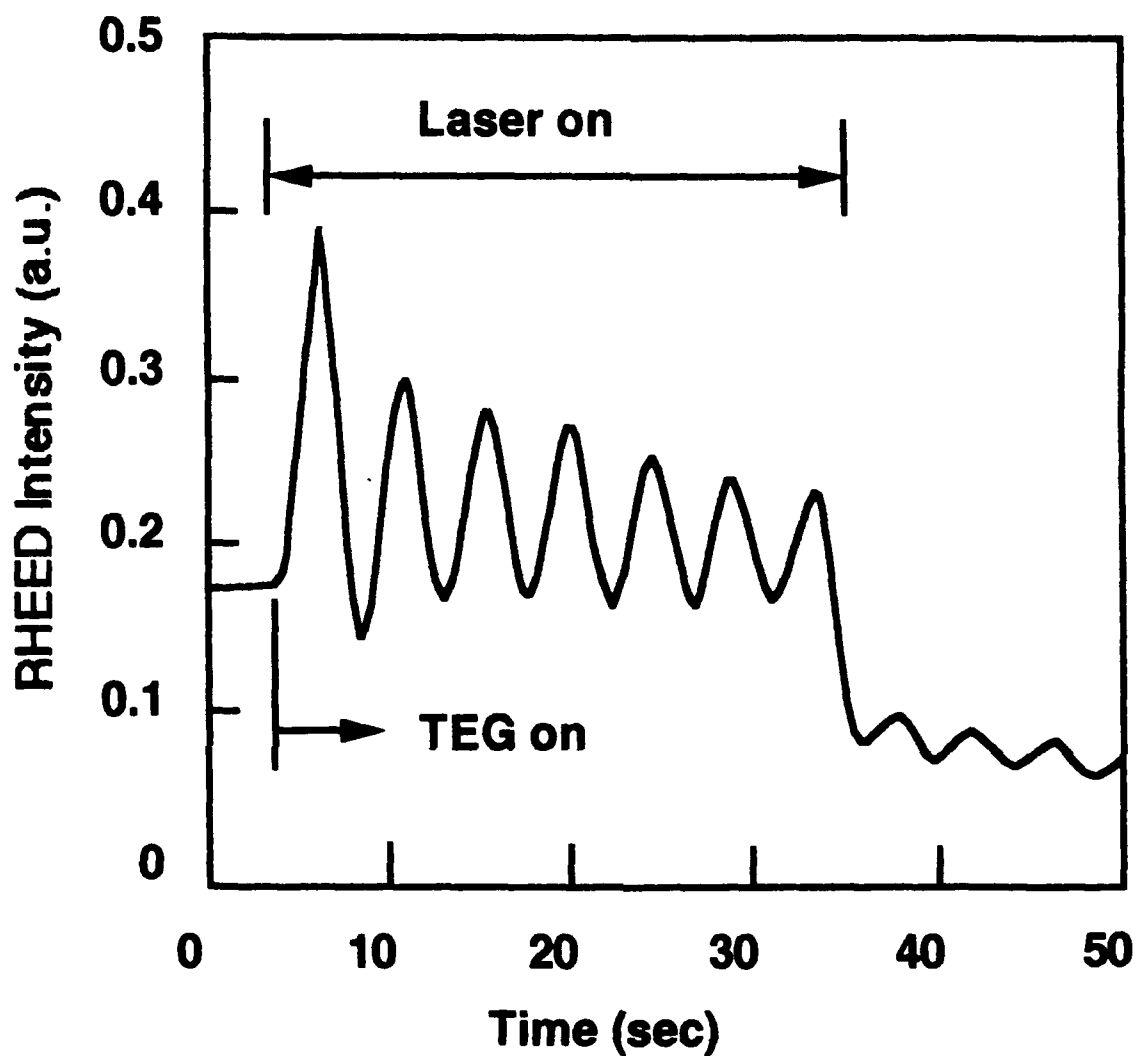


Fig. 21 RHEED oscillations with and without Ar ion laser irradiation with TEGa and As supply at a substrate temperature of 410°C

enhancement of growth rate with laser irradiation in comparison to that without laser irradiation becomes smaller with increasing substrate temperature, because the thermal decomposition of TEGa becomes more important.

2.3.2 Laser-Enhancement of Arsenic Desorption and its Effects

Fig. 22 shows the RHEED data of arsenic desorption behavior under 5-W Ar⁺ laser irradiation at a substrate temperature of 500°C. Only As₄ was used, and the arsenic cell shutter was always open during the study. The laser effect is clearly seen from the decrease of the RHEED intensity while the laser is turned on and from the recovery of the RHEED intensity while the laser is turned off. Similar behavior of RHEED data is obtained in studying the desorption of arsenic from GaAs without laser irradiation. In this case, we close the arsenic cell shutter (instead of turning on the laser) and then open the arsenic cell shutter (instead of turning off the laser). When we block the As₄ beam (although there may still be some flux leaked out), the surface arsenic concentration is lowered and the surface becomes rougher because of the desorption of arsenic from the heated surface so that the RHEED intensity decreases. When we restore the As₄ beam, the RHEED intensity recovers. The same kind of experiment is also done at lower substrate temperatures, and similar behavior, but with a smaller change of RHEED intensity, is observed. Therefore, we conclude that Ar⁺ laser irradiation enhances the desorption of arsenic.

In our previous MOMBE growth study, we have already found that group-III and group-V species are equally important in the surface chemical reactions [23]. The growth rate of GaAs changes with arsenic surface concentration, and growth can become arsenic-controlled if the arsenic surface concentration is low. In this case, increasing the arsenic flux results in increasing the growth rate. On the other hand, too high an arsenic concentration results in site blocking or enhanced desorption of TEGa molecules, and

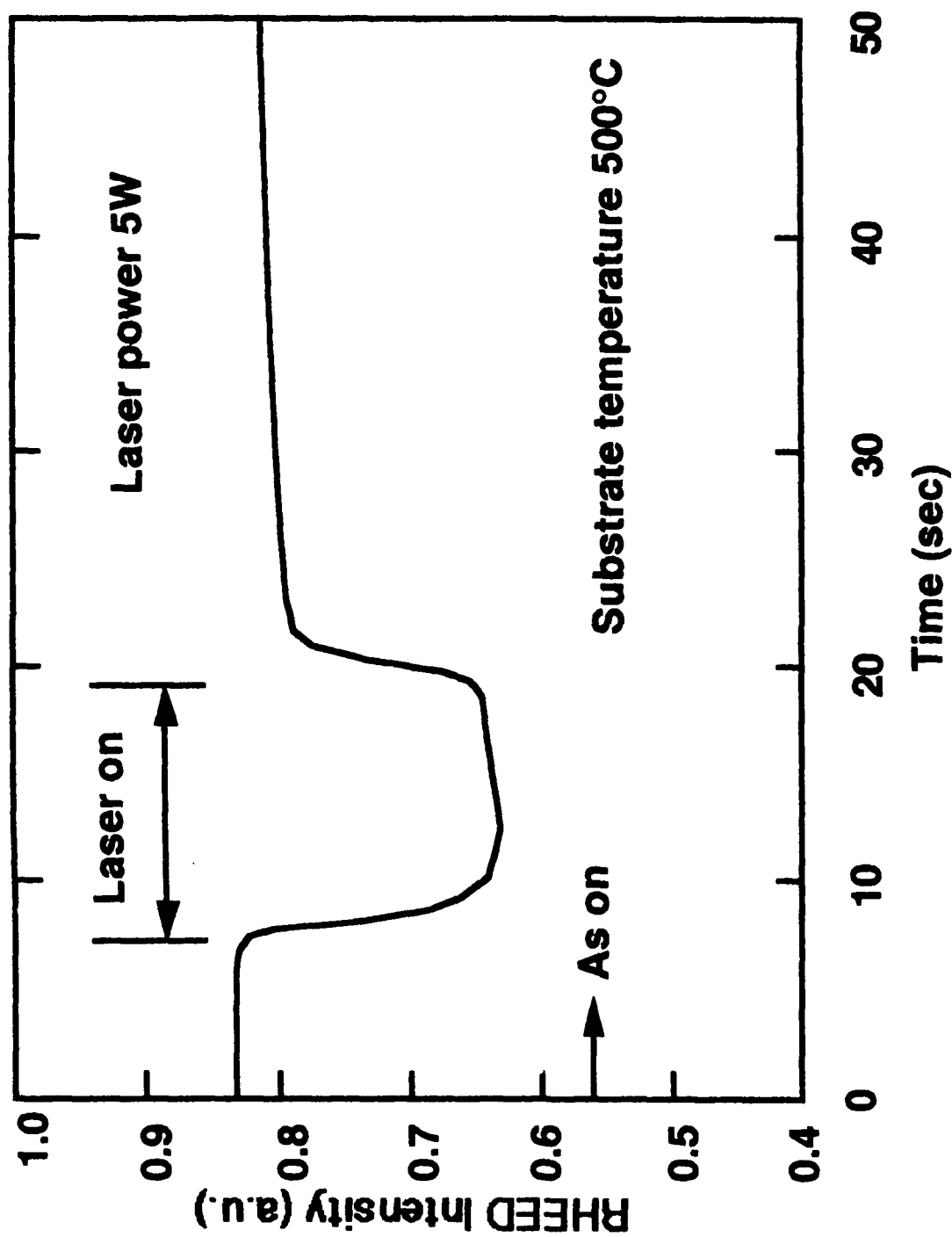


Fig. 22 RHEED data showing arsenic desorption behavior under laser irradiation and arsenic exposure

hence, lowers the growth rate. With Ar^+ laser irradiation, the arsenic surface concentration is decreased, resulting in a growth-rate change.

Figure 23 shows the growth rates as a function of the arsenic beam-equivalent pressure under 4-W Ar^+ laser irradiation at a substrate temperature of 390°C . These data are similar to the result obtained in the normal MOMBE growth of GaAs using TEGa and arsine and trimethylgallium (TMGa) and arsenic. The growth rate of GaAs changes with arsenic surface concentration, and growth can become arsenic-controlled. The growth rate decreases at high arsenic overpressure, because the site-blocking effect or the enhanced desorption of TEGa molecules lowers the TEGa coverage on the surface. The growth rate also decreases at lower arsenic pressure, because the rate-limiting step in the surface reaction forming GaAs involves the role of arsenic species and the growth is arsenic-controlled. Lower arsenic flux, or lower arsenic coverage on the surface, results in lower growth rate. Therefore, in laser-assisted MOMBE growth of GaAs, one cannot expect to obtain a desired growth rate by changing only the Ga flux without considering the arsenic effect. The V/III ratio is a crucial parameter in MOMBE and laser-assisted MOMBE growth.

In order to obtain a better understanding of the selective growth mechanism, we studied the relationship between the growth rate and the laser power. The results are shown in Fig. 24. The growth study was performed at a substrate temperature of 390°C with different arsenic fluxes, but the same TEGa flow, under different laser power. For arsenic flux values of 2.0×10^{-6} and 2.5×10^{-6} torr, the growth rate increases monotonically at low laser power and becomes saturated at high laser power. Both the decomposition rate of TEGa and the desorption rate of arsenic increase with increasing laser power. The decomposition of TEGa raises the growth rate, while the desorption of arsenic lowers the growth rate. As seen in the figure, the growth rate increases with increasing arsenic flux in the case with no laser irradiation, which indicates that we are in the arsenic-controlled growth regime. Fig. 23 also proves that we are in the arsenic-

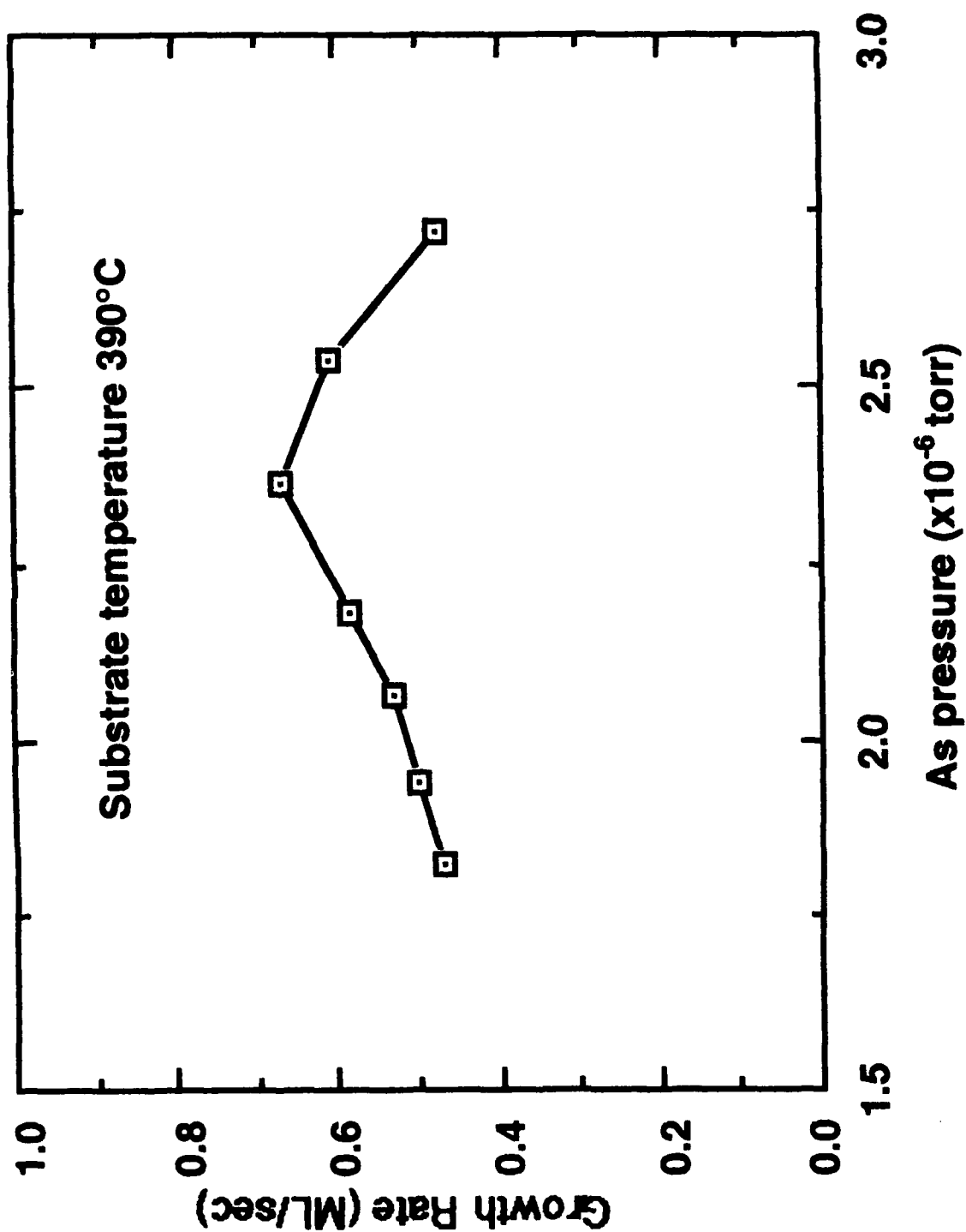


Fig. 23 The growth rate of GaAs versus arsenic beam equivalent pressure under 4-W Ar ion laser irradiation at a substrate temperature of 390°C

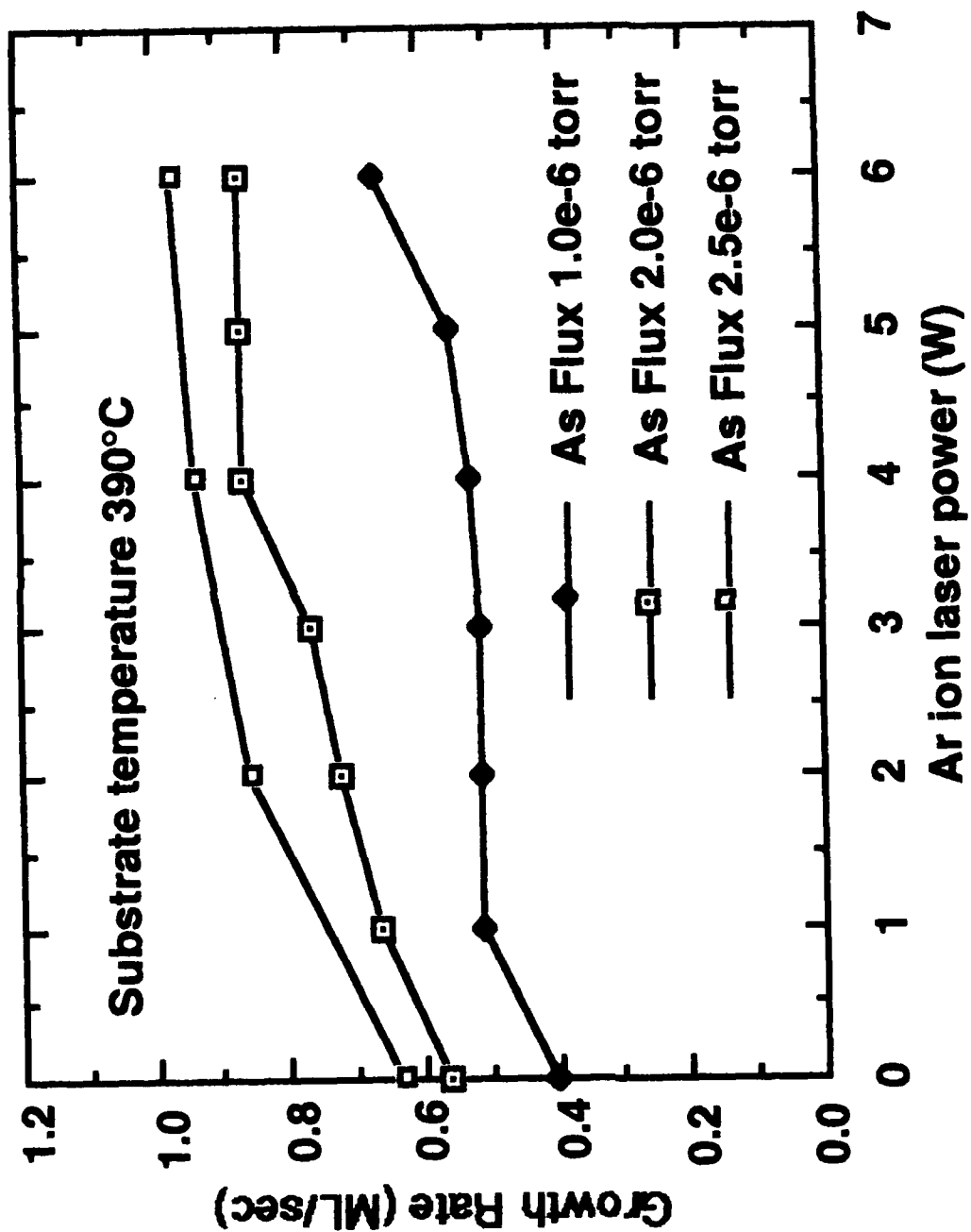


Fig. 24 Growth rate versus Ar ion laser power at constant TEGa flow but under different arsenic flux at a substrate temperature of 390°C

controlled growth regime during LAMOMBE growth of GaAs. From Fig. 8, we can clearly see that the arsenic thermal desorption from the substrate surface will become severe at high laser power (e.g., the surface temperature rise is over 100°C at 5-W laser power). At low laser power, the growth rate is mainly determined by the enhanced decomposition of TEGa, so the growth rate increases monotonically. At high laser power, arsenic desorption becomes severe and balances the decomposition of TEGa, so the growth rate becomes almost constant. Except for the case of 1.0×10^{-6} torr As_4 and 6-W laser power, which is not understood yet, this explanation of saturated growth rate seems correct.

From the above results, we see that Ar^+ laser-assisted MOMBE growth is a process in which decomposition of TEGa and desorption of arsenic compete with each other in the surface chemical reaction, resulting in saturation in enhanced growth rate in an arsenic-controlled growth regime.

2.3.3 The Initial Growth Behavior

From the RHEED oscillation data, we observed that the growth time of the first GaAs monolayer was quite different from that of the succeeding monolayers in the laser-assisted MOMBE growth. The initial growth behavior was studied by inspecting the growth time η of the first monolayer at different surface arsenic coverage. Figure 25 shows the relationship between η and laser power under three different arsenic fluxes at a substrate temperature of 390°C. Here, η decreases monotonically as laser power increases for each arsenic flux, and this may be attributed to the proportionality between the TEGa decomposition rate and the laser power. However, η is smaller for higher arsenic flux at low laser power (<4W) and for lower arsenic flux at high laser power (>4W). In our experiment, before the Ar^+ laser and TEGa were turned on synchronously, the arsenic flux had been turned on for 2 minutes and the substrate surface was covered by layers of arsenic adsorbates. These adsorbates include one

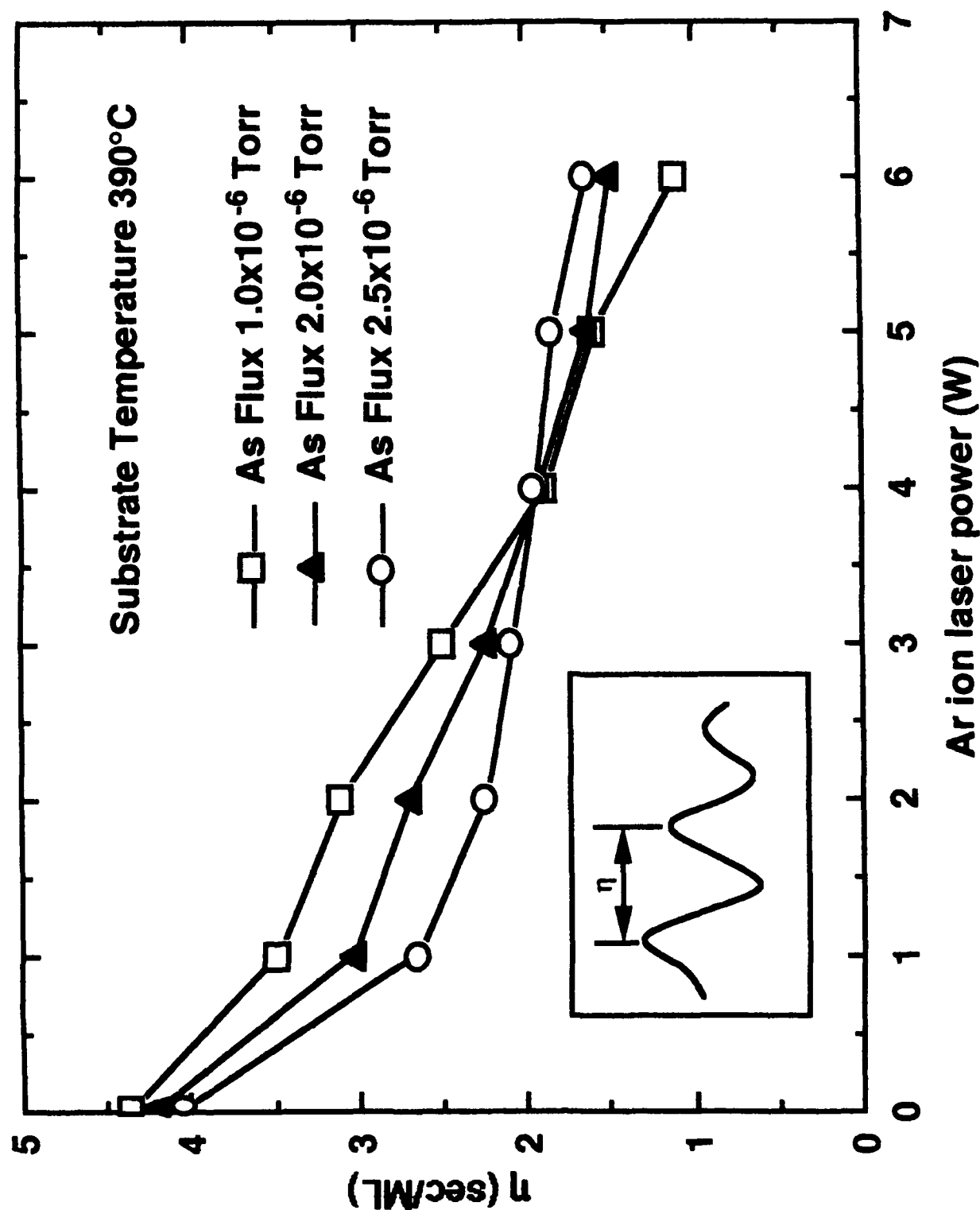


Fig. 25 The growth time of the first monolayer η versus the Ar ion laser power under three different arsenic fluxes at a substrate temperature of 390°C

monolayer of chemisorbed arsenic and several layers of physisorbed arsenic. The one monolayer Ga deposition can be on chemisorbed arsenic or physisorbed arsenic. At low laser power, the physisorbed arsenic atoms prevent the Ga atoms from reaching the chemisorbed arsenic atoms because of the low arsenic desorption rate, and hence the physisorbed mechanism prevails. The more physisorbed arsenic species on the surface, the more Ga adatoms are bounded on the physisorbed arsenic atoms, and so the higher arsenic flux results in faster Ga deposition or smaller η . At high laser power, most of the physisorbed arsenic atoms desorb from the sample surface, so the chemisorbed mechanism dominates. The remaining physisorbed arsenic atoms act as site-blocking centers, so the lower arsenic flux results in less site-blocking effect that leads to faster Ga deposition on chemisorbed arsenic atoms or smaller η . The two mechanisms compete with each other at intermediate laser power ($\approx 4\text{W}$), and this is seen from the intersection of η value for three different arsenic fluxes at 4-W laser power.

2.3.4 Postgrowth Characterization

The LAMOMBE grown samples were investigated under Nomarski microscope, SEM and the thickness was measured with a Dektak stylus profiler. Fig. 26 is the cross-section profile of the GaAs spot measured by a Dektak stylus profiler, and the growth rate measured is approximately the same as that monitored by the RHEED oscillations. We have also grown several LAMOMBE InAs sample (the lowest growth temperature is 200°C), but we did not observe any enhanced growth by both *in situ* and *ex situ* measurement.

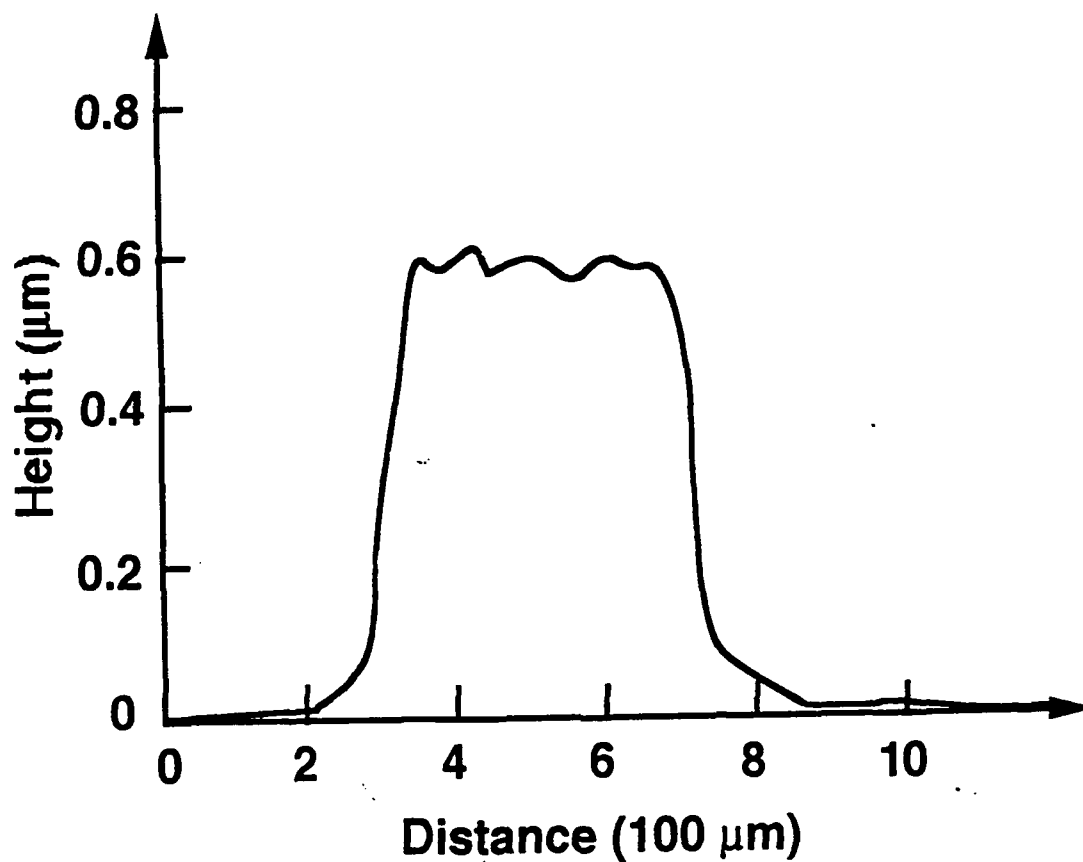


Fig. 26 The cross section profile of the GaAs spot measured by Dektak stylus profiler

3. FUTURE WORK

The present CBE system, as shown in Fig. 27, evolved from the original solid source Perkin Elmer 425B MBE system. The group III metalorganic gas lines, including TEGa, TMIn and trimethylaluminum (TMAI), have been installed to the system with a run/vent manifold controlled by pneumatic valves. The lines are connected to the system through effusion cell ports and the gas flow is controlled by MKS 1150B vapor source mass flow controllers (2 sccm full scale). The group-V lines are more complicated because of safety measures for toxic gases, but they will be ready at the end of February, 1993. The doping line will be ready for use at the end of March, 1993, and the gas flow will be controlled by a combination of baratrons and leak valves.

The reason for building new gas lines is for computer control, which is essential for growing heterostructures reproducibly. In order to enhance the system pumping capability, we have installed a 1500 l/s turbo pump and a 2200 l/s cryopump. The turbo pump pumps mainly the metalorganics, while the cryopump pumps mainly the hydrogen. The system is equipped with a quadruple mass spectrometer and a RHEED gun. The Argon ion laser is focused down to 400 mm and directed to the sample through the central pyrometer viewport. A computer-controlled scanning mirror set was installed to scan the laser beam.

As to the growth study, we shall investigate patterned growth by laser scanning and characterize these samples by various electrical and optical measurements. We shall concentrate on phosphorous-related materials and study MOMBE and LAMOMBE of mixed group-V compounds as well as selective-area doping.

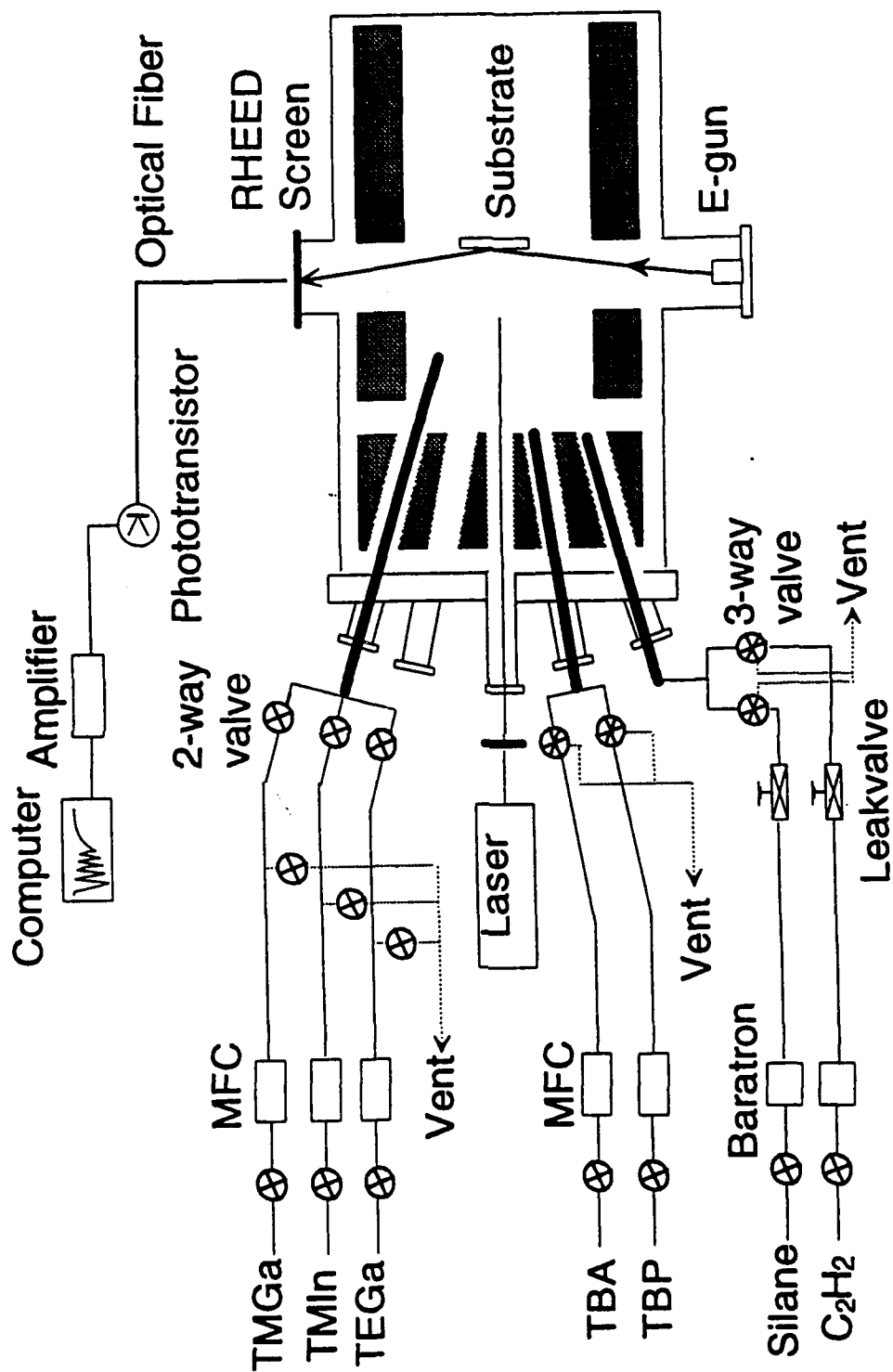


Fig. 27 LAMOMBE system

4. REFERENCES

- [1] C. M. Gronet, J. C. Sturm, K.E. Willians, J. F. Gibbons, and S. D. Wilson, Appl. Phy. Lett. **48**, 1012 (1986)
- [2] W. Heimann and U. Mester, Inst. Physics. Conf. Ser. No. **26**, 219 (1975)
- [3] C. F. Warnke, in Temperature: Its Measurement and Control in Industry, edited by H. H. Plumb (Instrument Society of America, Pittsburgh, 1975), Vol. 4
- [4] James F. Schooley, Thermometry, Chemical Rubber, Cleveland, OH, 1986
- [5] V. M. Donnelly and J. A. McCaulley. J. Vac. Sci. Technol. **A8**, 84 (1990)
- [6] H. Sankur and W. Gunning. Appl. Phys. Lett. **56**, 2651 (1990)
- [7] E. A. Morozova, G. A. Shafeev and M. Wautelet. Meas. Sci. Technol. **3**, 302 (1992)
- [8] Katherine L. Saenger and Julie Gupta. Applied Optics **30**, 1221 (1991)
- [9] James C. Sturm. Casper M. Reaves. IEEE Trans. on Electron Devices **39**, 81 (1992)
- [10] F.G. Allen, Silicon Molecular Beam Epitaxy, edited by J. C. Beam (Electrochemical Society, Pennington, N. J., 1985), pp.3-15.
- [11] Glen E. Myers, Analytical Methods in Conduction Heat Transfer, pp.1-33.
- [12] B.W.Liang and C.W.Tu, Appl. Phys. Lett. **57**, 689(1990)
- [13] B. W. Liang, T. P. Chin and C. W. Tu, J. Appl. Phys. **67**, 4393 (1990)
- [14] T. H. Chiu, J. E. Cunningham and A. Robertson, J. Crystal Growth **95**, 136(1989)
- [15] D. E. Lacklison, C. T. Foxon, J. Zhang, B. A. Joyce and E. M Gibson, J. Crystal growth **120**, 50 (1992)
- [16] E. T. FitzGerald, C. L. French and J. S. Foord, J. Crystal Growth **120**, 57 (1992)
- [17] Y. Iimura, K. Nagata, Y. Aoyagi, S. Namba, J. Crystal Growth **105**, 230 (1990)
- [18] N. Kobayashi, J. L. Benchimol, F. Alexandre and Y. Gao, Appl. Phys. Lett. **51**, 1907 (1987)
- [19] H. Sugiura, R. Iga and T. Yamada, J. Crystal Growth **120**, 389 (1992)

- [20] T. Yamada, R. Iga, H. Sugiura, Appl. Phys. Lett. **61**, 2449 (1992)
- [21] V.M.Donnelly, C.W.Tu, J.C.Beggy, V.R.McCrary, M.G.Lamont, T.D.Harris,
F.A.Baiocchi and R.C.Farrow, Appl. Phys. Lett. **52**, 1065 (1988)
- [22] Y.Aoyagi, M.Kanazawa, A.Doi, S.Iwai and S.Namba, J. Appl. Phys. **60**, 3131
(1986)
- [23] K.Nagata, Y.Iimura, Y.Aoyagi, S.Namba and S.Den, J. Crystal Growth **105**, 52
(1990)
- [24] Y.Aoyagi, T.Meguro, S.Iwai and A.Doi, Mater. Sci. & Engi. **B10**, 121 (1991)
- [25] H.Sugiura, T.Yamada and R.Iga, Jpn. J. Appl. Phys. **29**, L1 (1990)
- [26] H.Sugiura, R.Iga, T.Yamada and M.Yamaguchi, Appl. Phys. Lett. **54**, 335 (1989)
- [27] R.Iga, H.Sugiura, T.Yamada and K.Wada, Appl. Phys. Lett. **55**, 451 (1989)
- [28] R.Iga, H.Sugiura and T.Yamada, Jpn. J. Appl. Phys. **29**, 475(1990)
- [29] R.Iga, H.Sugiura and T.Yamada, Jpn. J. Appl. Phys. **30**, L4 (1991)
- [30] Y.I.Nissim, A.Lietoila, R.B.Gold and J.F.Gibbons, J. Appl. Phys. **51**, 274 (1980)
- [31] H. K. Dong, B. W. Liang, M. C. Ho, S. Hung and C. W. Tu, J. Crystal Growth **124**,
181 (1992)